Renewable Energy 146 (2020) 223–241

Contents lists available at ScienceDirect

Renewable Energy

journal homepage: www.elsevier.com/locate/renene

Calculating wind turbine component loads for improved life prediction

D.P. Rommel*, D. Di Maio, T. Tinga

University of Twente, Mechanics of Solids, Surfaces and Systems Department, Enschede, 7522 NB, the Netherlands

ARTICLE INFO

Article history:
Received 7 December 2018
Received in revised form
9 May 2019
Accepted 21 June 2019
Available online 26 June 2019

Keywords:
Load based maintenance
Physical model
Wind turbine
Rotor loads
Aerodynamic imbalance

ABSTRACT

Wind turbines life time is commonly predicted based on statistical methods. However, the success of statistics-based maintenance depends on the amount of variation in the system design, usage and load. Life time prediction based on physical models seeks to overcome this drawback by considering the actual design and evaluating the specific usage, load and operating condition of the considered systems. In this paper, a load-based maintenance approach is proposed to predict wind turbines life time. Physical models are used to evaluate load profiles at wind turbine blade root, rotor hub center and tower head. The effects of surface roughness, side winds, yaw misalignment, rotor tilt and blade cone angle, individual blade pitching and wind turbulences are considered and quantified. It is shown that centrifugal, gravity, Euler and Coriolis accelerations dominate the blade root loads. Tilt and cone angle, as well as individual blade pitching, affect the rotor hub and dynamic tower head loads. Further, the actual wind speed distribution is considered which is also proven to be a critical life time prediction parameter. Finally, a set of parameters is proposed that need to be monitored in a specific wind turbine to enable the practical implementation of a predictive maintenance policy.

© 2019 The Authors. Published by Elsevier Ltd. This is an open access article under the CC BY license (http://creativecommons.org/licenses/by/4.0/).

1. Introduction

It is expected that installation, operation and maintenance (O&M) costs in offshore wind parks are nearly one-third of the levelized cost of energy [1]. Thus, reducing O&M costs has a significant contribution to lower levelized cost of energy. Furthermore, unplanned failures of wind turbine systems cause the majority of O&M costs of offshore wind farms [2]. Therefore, failure prediction is essential to efficiently plan maintenance activities in advance and thus, to reduce the O&M costs. Failures of wind turbine systems are commonly predicted based on failure statistics [3] which, are used for planning maintenance activities [4]. Other approaches follow data driven or model-based methods for failure prediction. Data driven methods or big data frameworks [5] directly use condition monitoring or SCADA data [6] in combination with prognostics methods like Bayesian probability theory [7,8], Wiener process [9] or artificial neural networks [10,11] to evaluate the remaining useful life (RUL). Model-based methods utilize, for example, physics of failure [12,13] to predict failures and calculate the life time of components. Note that some model-based methods are inspired by physical principles, but are statistics-based in reality. This means that a lot of approaches of life time prediction proposed in literature are statistics-based. However, statistics-based maintenance is less precise than model-based-maintenance [14], especially when large variations in design, loads or operating conditions occur, as it is typical for wind turbines. As these variations cannot be adequately incorporated in statistics-based methods, this leads to large uncertainties in life predictions and conservative maintenance intervals [13]. Consequently, the accuracy of life time prediction can be increased by a model-based approach which uses purely physical equations and calculations. Djeziri et al. [15] propose a hybrid method for the prediction of the RUL in order to not apply statistics-based methods. Thereby, a wind turbine model and measurements at a real wind turbine are combined. The model simulates the system behavior under normal and faulty condition, e.g. bearing failure. The RUL is evaluated by comparing the measured and simulated, normal and faulty conditions. This means also that Djeziri et al. [15] follow the approach of condition based maintenance where maintenance decisions are based on measurements of system performance or degradation. The closer the measured condition is known to the faulty condition, the shorter is the RUL.

* Corresponding author.
E-mail address: d.p.rommel@utwente.nl (D.P. Rommel).

https://doi.org/10.1016/j.renene.2019.06.131
0960-1481/© 2019 The Authors. Published by Elsevier Ltd. This is an open access article under the CC BY license (http://creativecommons.org/licenses/by/4.0/).

Nomenclature

A	area, [m^2]
A	Amplitude
a	axial intereference factor
a	acceleration, [m/s^2]
a'	tangential intereference factor
a,b,c,d,e	polynomial constants
B	number of blades, bearing
b	bending
bl	blade
c	chord length, [m]
C_l	lift coefficient
C_d	drag coefficient
C_n	C_l and C_d normal to rotor plane
C_t	C_l and C_d tangential to rotor plane
cog	center of gravity
F_l	lift force, [N]
F_d	drag force, [N]
F_n	force normal to rotor plane, [N]
F_t	force tangential to rotor plane, [N]
F_r	force radial to rotor plane, [N]
F_{bl}	force at blade root, [N]
F, f	Prandtl correction factor
g	gravity acceleration, [m/s^2]
H	hub
HB	hub - bearing
i,j,k	Factors, counters
l	length, distance, [m]
L_B	force at pitch/main bearing, [N]
L_{eq}	equivalent bearing load, [N]
L_{10}	bearing life time, [h]
M_n	moment around normal axis, [Nm]
M_t	moment around tangential axis, [Nm]
M_r	moment around radial axis, [Nm]
$M_{a.f.}$	airfoil twist moment, [Nm]
M_{bl}	moment at blade root, [Nm]
m	mass, [kg]
P	power, [W]
r	(local) blade radius, [m]
R	blade tip radius, [m]
R_{cog}	Blade radius of center of gravity, [m]
u	circumferencial speed, [m/s]
v, v_w	speed, wind speed, [m/s]
V	volume, [m^3]
w	relative speed, [m/s]
α	[°] angle of attack
β	blade twist/pitch angle, [°]
γ	rotor tilt angle, [°]
Γ	circulation, [m^2/s]
δ	blade cone angle, [°]
ε	side (shear) wind angle, [°]
λ	tip speed ratio
μ	non-dimensional radius
ρ	air density, [kg/m^3]
σ	solidity, [m]
φ	angle of relative wind, [°]
φ^*	modified angle of relative wind, [°]
χ	blade tilt angle, [°]
ψ	rotating angle of rotor, [°]
ω	angular speed, [1/s]
rtn/r't'n'	rotating coordinates (rotor/blade), radial, tangential, normal
xyz/x'y'z'	initial coordinates (rotor/main shaft)

In this paper a load-based maintenance approach is proposed to utilize the model-based methods based on purely physical equations. Load and usage-based maintenance policies have already been proposed and applied by Tinga [13]. For usage-based maintenance, he proposed to translate the system usage (on the global level) to the local (internal) loads like stress, strain or temperature. But, in mechanical systems these local loads can also be retrieved from the forces and moments (global loads) acting on or inside the mechanical system. Consequently, load-based maintenance can be executed by evaluating the global loads of the mechanical system as it will be shown in the present paper. Using load-based maintenance instead of condition-based maintenance provides the advantage that the RUL can already be predicted when the system is still "healthy", i.e. at a stage where the real system still runs at or close to (simulated) normal condition and degradation cannot be measured yet. Further, load profiles, i.e. the range of loads a specific components is subjected to, do not depend on time rather on operational and environmental conditions. If the system has, at least once, run through the range of operational and environmental conditions, then the load profile is known and the life time can be predicted from a (measured or assumed) combination of these conditions. Moreover, it is important to note that the proposed load-based maintenance policy uses actual loads and load profiles which can differ from the loads and load profiles assumed during system design. This means that load-based maintenance has the potential to predict the system life time more accurately than as it is evaluated during the system design procedure. In addition, the evaluated actual load profile can also be used for improving new system designs by closing the design feedback loop. Scientific literature on such a load-based maintenance approach appears to be very limited, and no application in wind turbines could be found at all. Thus, the objectives of this paper are i) to propose the general concept of load calculations that can feed into a load-based maintenance approach and ii) specifically develop a method for wind turbine components.

Before applying the approach of load-based maintenance, the physical models used for global load evaluations must be specified. Firstly, it is important to note that global loads, i.e. forces and moments, are dependent on the design (specific geometries), operation and environment of the considered system. Hence, the physical model used for global load calculations must, on the one hand, be based on a design model and, on the other hand, consider the actual (measured) operational and environmental conditions. This means that the algorithms behind the physical design model must be able to handle measurements, ideally in real time operation. A design model is a numerical model that is used for a range of calculations during the design process, like calculation of loads, life time or performance. The results govern design choices on materials and dimensions. Secondly, load-based maintenance requires a detailed analysis of loads and system behavior to select the most dominant influences of design, operation and environment on the system load profiles. The dominant effects must, at least, be incorporated in the life time prediction. Summing up, the physical model used for the global load calculation must describe the system design, operate in real time and be able to easily analyze the system behavior. After Gokhale and Trivedi [16] an analytical model fits best to these requirements.

The approach of (global) load-based maintenance is applied in

this paper to a three bladed, horizontal axis wind turbine. Thereby, the global load evaluation focuses on the wind turbine rotor because rotor loads have a significant influence on the life time of the entire wind turbine, namely on the life time of blades, pitch-, yaw- and main power train as well as the tower. The rotor and blades are described by an analytical design model. On the one hand, the design model provides, based on simple blade design data, a virtual copy of the real wind turbine rotor. On the other hand, the design model is used, after some model modifications, to evaluate load profiles based on measured operational and environmental data. This means that for every specific wind turbine the load profiles of the wind turbine rotor can be calculated individually and hence, also the life time.

The main scientific contribution of this work is the proposal of a novel load-based maintenance approach for wind turbine components, quantifying the loading of a component (and associated expected service life) from a combination of a component-specific physical model (the design model) and the actual (measured) operational and environmental conditions. The additional practical contribution is the implementation of the approach for a wind turbine rotor, demonstrating the dominant factors (and their magnitude) affecting the blade, hub and tower loads (and life time).

The outline of the paper is as follows: in section 2 the physical model for quantifying the rotor loads is derived. First a basic rotor model is developed, also including a basic blade design procedure (as commonly not all blade details are available). Then the effects of a range of variations are included in the model and the calculation procedure is discussed. Section 3 then applies the model to the case of a 3 bladed wind turbine rotor, demonstrating and discussing the qualitative results of variations in operational conditions. Section 4 focuses on the verification of the model results and contains a critical discussion. Finally, section 5 forwards the main conclusions of the work.

2. Wind turbine rotor load calculation

This section presents the analytical models which are needed for the rotor load calculations under real time conditions. In total two models are required. One model is used for the design of the virtual wind turbine rotor, i.e. the geometry of the wind turbine rotor. This is necessary as the detailed geometry of the rotor is in most cases not available. A second model evaluates the wind turbine rotor loads during operation based on the geometry of the virtual wind turbine rotor and measurements. The second model builds on the first model and is additionally enriched with effects, which influence the rotor behavior and loads during operation. The effects that are considered in the present paper are: wind profile over height (surface roughness), yaw misalignment and side winds, tilt and cone angle as well as tower displacement, individual blade pitching and, wind turbulences. Some equations implemented in the second model can lose their mathematical validity at specific operating conditions. These calculation limits are discussed at the end of this section.

2.1. Analytical blade model of virtual rotor

A model of a three bladed wind turbine rotor can easily be created by triplicating the model of one turbine blade. The Blade Element Momentum (BEM) theory provides a set of equations to analytically describe the transfer of fluid flow properties (wind) into the motion and loading of a wind turbine blade. In the BEM theory the turbine blade is divided into sections. Then, a set of analytical equations is defined for every blade section. A complete derivation of the BEM theory is beyond the scope of this paper. Therefore, only those equations are mentioned here which are needed for the calculation procedures. Detailed descriptions of the BEM theory are given by Refs. [17–19]. Nevertheless, two crucial points of the BEM theory shall be highlighted here.

First, the BEM theory adopts two main assumptions for every blade section: a) energy contained in the wind speed can only partially be converted to mechanical rotating energy of the turbine rotor and b) the angular rotor speed increases due to wake, i.e. due to the momentum caused by the wind on the blade surface while changing wind direction in the turbine rotor. Effect a) is expressed by an axial interference factor a and effect b) by a tangential interference factor a' [17]. Fig. 1 shows the speed triangle including axial and tangential interference factors as well as aerodynamic forces at an airfoil (blade section). The actual wind speed v_w is scaled by the axial interference factor a and the rotor circumferential speed u by the tangential interference factor a'. Together these determine the relative wind speed w_{rel} that the airfoil is exposed to (also defined by angle φ). As a result, the lift force F_l and drag force F_d are generated, which can be decomposed into a normal (F_n) and tangential (F_t) force that cause blade bending and rotor rotation. The interference factors will be defined in detail below.

Second, in an extended version of the BEM theory air flow losses at the blade tip and root can be included by the Prandtl correction factor F respectively f_{root} and f_{tip} [19]. The losses are caused by a radial airflow due to the pressure difference between suction and pressure side of the blade [19]. In order to minimize these losses, the circulation Γ around the airfoil at the blade ends is set to zero during the blade design process which is also done by the Prandtl correction factors as shown later. Finally, after [17–19] the set of equations for a simple blade design are given as:

Axial interference factor

$$\text{if } a \le a_c \qquad a = \frac{1}{\frac{4\sin^2(\phi)}{\sigma C_n} + 1} \tag{1a}$$

$$\text{if } a > a_c \qquad a = \frac{1}{2}(2 + K(1 - a_c) \times) - \frac{1}{2}\sqrt{(K(1-2a_c)+2)^2 + 4(Ka_c^2 - 1)} \tag{1b}$$

with $K = \frac{4\sin^2(\phi)}{\sigma C_n}$.

Note that the simple BEM theory (Eq. (1a)) is only valid for small values of a, and breaks down at $a_c = 0.2$ [17,18]. Therefore, the axial interference factor a must be calculated after Eq. (1b) if $a > a_c$.

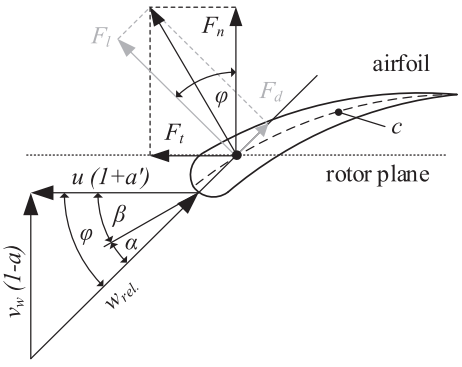

Fig. 1. Wind speed triangle and aerodynamic forces at airfoil.

Tangential interference factor

$$a' = \frac{1}{\frac{4F\,\sin(\phi)\cos(\phi)}{\sigma C_t} - 1} \tag{2}$$

In the expressions for the two interference factors the following parameters are used:

– the angle of relative wind w.r.t rotor plane φ (cp. Fig. 1):

$$\tan(\phi) = \frac{(1-a)}{(1+a')}\frac{1}{\mu\lambda} \tag{3}$$

– the tip speed ratio λ which is the ratio of the circumferential rotor speed at the blade tip and the wind speed:

$$\lambda = \frac{u_{tip}}{v_w} = \frac{\omega R}{v_w} \tag{4}$$

– the non-dimensional blade radius which is defined by the local blade radius r of the different blade sections and the maximum blade radius R, i.e. $\mu\ \varepsilon\ [0;1]$:

$$\mu = \frac{r}{R} \tag{5}$$

– the solidity which is the ratio of the local blade (airfoil) area and local rotor area. The airfoil area is given by the airfoil chord length c, the difference of local blade radii Δr and the number of blades B:

$$\sigma = \frac{c\Delta r B}{2\pi r \Delta r} = \frac{cB}{2\pi r} \tag{6}$$

– the projected lift and drag coefficient normal (C_n) and tangential (C_t) to rotor plane with C_l and C_d the airfoil lift and drag coefficients (cp. also the projection of lift (F_l) and drag (F_d) force to a tangential (F_t) and normal (F_n) force in Fig. 1):

$$C_n = C_l\cos(\phi) + C_d\sin(\phi) \tag{7a}$$

$$C_t = C_l\sin(\phi) - C_d\cos(\phi) \tag{7b}$$

– the Prandtl correction factor:

$$F = f_{root}f_{tip} \tag{8}$$

– the Prandtl correction factor components at blade root and tip:

$$f_{root} = \frac{2}{\pi}\cos^{-1}\left(\exp\left(-\frac{B}{2\sin(\phi)}\frac{(\mu-\mu_{root})}{\mu}\right)\right) \tag{8a}$$

$$f_{tip} = \frac{2}{\pi}\cos^{-1}\left(\exp\left(-\frac{B}{2\sin(\phi)}\frac{(1-\mu)}{\mu}\right)\right) \tag{8b}$$

The BEM theory is normally applied to calculate the optimal chord c for new blade designs. However, for a virtual wind turbine rotor, i.e. a copy of an existing wind turbine rotor, the chord is already defined. So two assumptions are made here: first, the maximum chord of the blade (along it's span) is known from a blade data sheet and second, the circulation around the blade is constant along the blade radius ($\Gamma = const.$) except at blade tip and root where the circulation must be zero. Further, the consideration of the lift force provides a useful relation to describe the chord length c depending on the blade circulation, lift coefficient and relative wind speed. The lift force per blade length unit is specified by Ref. [17] as $F_l = \frac{\rho}{2}w_{rel.}^2 cC_l = \rho w_{rel.}\Gamma$ and thus, the chord length can be derived as $c = \frac{2\Gamma}{C_l w_{rel.}}$.

Based on the BEM theory an expression for a uniform circulation Γ along the blade radius including Prandtl correction factors is given by Ref. [19] as $\Gamma = \frac{4\pi}{\lambda}\frac{a}{(1-a)}F(1-Fa)^2$. From this equation, it can be seen that the circulation is only uniform along the blade radius, if the axial interference factor a is uniform, too. So it can be concluded that in this case (under the assumptions as defined before) the axial interference factor will be constant over the blade radius and the circulation at the blade root and tip only depends on the Prandtl correction factors. Furthermore, based on Fig. 1 the relative wind speed is defined as

$$w_{rel.} = \frac{v_w(1-a)}{\sin(\phi)} \tag{9}$$

So the chord length variation along the blade for a blade with uniform circulation (and constant axial interference factor) is given as a function of the non-dimensional radius by:

$$c(\mu) \sim \frac{F(\mu)[1-F(\mu)a]^2}{C_l(\mu)}\sin[\varphi(\mu)] \tag{10a}$$

Normally, variables like wind speed, interference factor etc. at the blade design point of the considered wind turbine are not available. Thus, the magnitude of the chord length at the different blade sections cannot be evaluated. However, the value of the maximum chord length $c_{max.ref.}$ is often given in the blade data sheet. Then, the blade chord lengths can be calculated by scaling Eq. (10a) with the ratio of the given chord length maxima. Hence, the chord length c along the blade radius can be described for the virtual rotor as follows:

$$c(\mu) = \frac{c_{\max.ref.}}{[\max(c(\mu))]_{Eq.10a}}\frac{F(\mu)[1-F(\mu)a]^2}{C_l(\mu)}\sin[\varphi(\mu)] \tag{10b}$$

The chord length calculated after Eq. (10b) can be used in Eq. (6). Then, Eqs. (1)–(8) can be solved for given lift and drag coefficients, i.e. for given airfoils resulting in the actual values of the interference factors a and a', and the resulting relative wind speed $w_{rel.}$ Furthermore, for given lift and drag coefficients as well as chord lengths the normal and tangential blade forces can be calculated (cp. also Fig. 1) and thus, also the blade thrust force, blade bending moments and rotor power [18].

Normal and tangential blade force (per unit blade length)

$$F_n^m = \frac{\rho}{2}w_{rel.}^2 cC_n \tag{11}$$

$$F_t^m = \frac{\rho}{2}w_{rel.}^2 cC_t \tag{12}$$

Table 1
Euros 100 – blade data.

Quantity	Unit	Value
Rotor diameter (approx.)	[m]	100
Rated power	[kW]	3000
Nominal wind speed	[m/s]	12.3
Mass	[kg]	12200
Design tip speed ratio	-	8.2
Max. chord length	[m]	4.15

Blade thrust force

$$F_n = R \int_{\mu_{root}}^{1} F_n^m d\mu \tag{13}$$

Blade bending moments around normal and tangential axis

$$M_t = R^2 \int_{\mu_{root}}^{1} F_n^m \mu d\mu \tag{14}$$

$$M_n = R^2 \int_{\mu_{root}}^{1} F_t^m \mu d\mu \tag{15}$$

Rotor power

$$P_{rotor} = \sum_{i=1}^{B} (M_n)_i \omega \tag{16}$$

Note that Eq. (11)–(16) are used for both evaluating the blade design of the wind turbine rotor and for calculating the wind turbine rotor loads during operation. The blade design as well as load calculation procedures are explained in the following subsections.

2.2. Blade design procedure of virtual rotor

The set of analytical equations is now used to design the blades of the virtual wind turbine rotor based on a real turbine blade. In order to do so, the blade EUROS 100 is chosen [20] in the present paper. Table 1 shows an extract from the data sheet of the blade EUROS 100.

Furthermore, after EUROS [20] the design of the blade EUROS 100 is based on the airfoils types DU and NACA 64. Therefore, in the present paper it is assumed for the blade design that the airfoil DU 97-W-300LM is used at the blade root region, DU 93-W-210LM around the blade center and NACA 64-618 at the blade tip region (cp. also Table 2). Then, the optimal angle of attack of these airfoils is calculated based on given lift and drag coefficients [21]. The optimal angle of attack is used for the blade design and is defined by the maximum value of the glide ratio (lift/drag ratio). Table 2 shows the values of angle of attack, lift and drag coefficient at chosen non-dimensional radii used for the blade design of the virtual wind turbine rotor. Based on Table 2 lift and drag coefficients as well as angle of attacks for all other non-dimensional blade radii $\mu \in [0.05, 1.0]$ are interpolated by fifth order polynomials.

Table 2
Blade design values.

Airfoil Type	Lift coefficient	Drag coefficient	Angle of attack [°]	Radius μ
DU 97-W-300LM	1.254	0.01116	7.5	0.05
DU 97-W-300LM	1.254	0.01116	7.5	0.1
DU 93-W-210LM	0.948	0.00664	3.5	0.5
NACA 64-618	1.001	0.00581	5	0.9
NACA 64-618	1.001	0.00581	5	1.0

Table 3
Polynomial constants for a blade after Table 2.

Polynomial Constant	Lift coefficient	Drag coefficient	Angle of attack
a	−5.250	−0.0540	−77.68
b	11.495	0.1268	166.8
c	−7.373	−0.0890	−104.0
d	0.915	0.0112	12.83
e	1.225	0.0108	7.098

$$C_l(\mu) = a_l\mu^4 + b_l\mu^3 + c_l\mu^2 + d_l\mu + e_l \tag{17}$$

$$C_d(\mu) = a_d\mu^4 + b_d\mu^3 + c_d\mu^2 + d_d\mu + e_d \tag{18}$$

$$\alpha(\mu) = a_\alpha\mu^4 + b_\alpha\mu^3 + c_\alpha\mu^2 + d_\alpha\mu + e_\alpha \tag{19}$$

The polynomial constants of Eq. (17)–(19) evaluated for the blade design after Table 2 are shown in Table 3. For the load calculation, it shall be noted here that polynomial constants of Eq. (17)–(19) must be re-evaluated as soon as lift, drag coefficient or angle of attack changes during operation. Fig. 2 shows the distribution of angle of attack, lift and drag value along the non-dimensional blade radius based on Tables 2 and 3 as well as Eq. (17)–(19). The lift and drag coefficient evaluation as a function of the non-dimensional radius is necessary to proceed the calculation as proposed in section 2.1. Then, the virtual wind turbine rotor is described by the set of equations of section 2.1 and the values of Tables 1–3.

As the interference factors and the angle of relative wind are independent (cp. Eqs. (1a), (1b) and (2) and 3), an iterative calculation procedure is needed. The design evaluation procedure of the virtual wind turbine rotor is visualized in Fig. 3. One can see that forces, moments and power are calculated at the end of the calculation procedure. The forces, moments and power evaluated at the blade design point can be used to compare the virtual and real wind turbine rotor. Here it is important to remember that the usage of the BEM theory is an approximation of the real blade design. So it can occur that the calculated power at the design point deviates

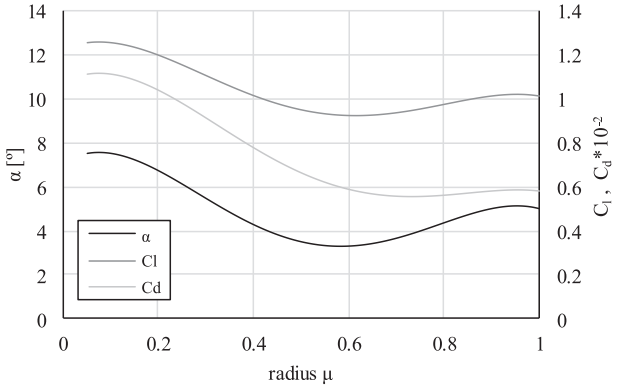

Fig. 2. Angle of attack, lift and drag coefficients along blade radius as estimated for the selected blade EUROS 100.

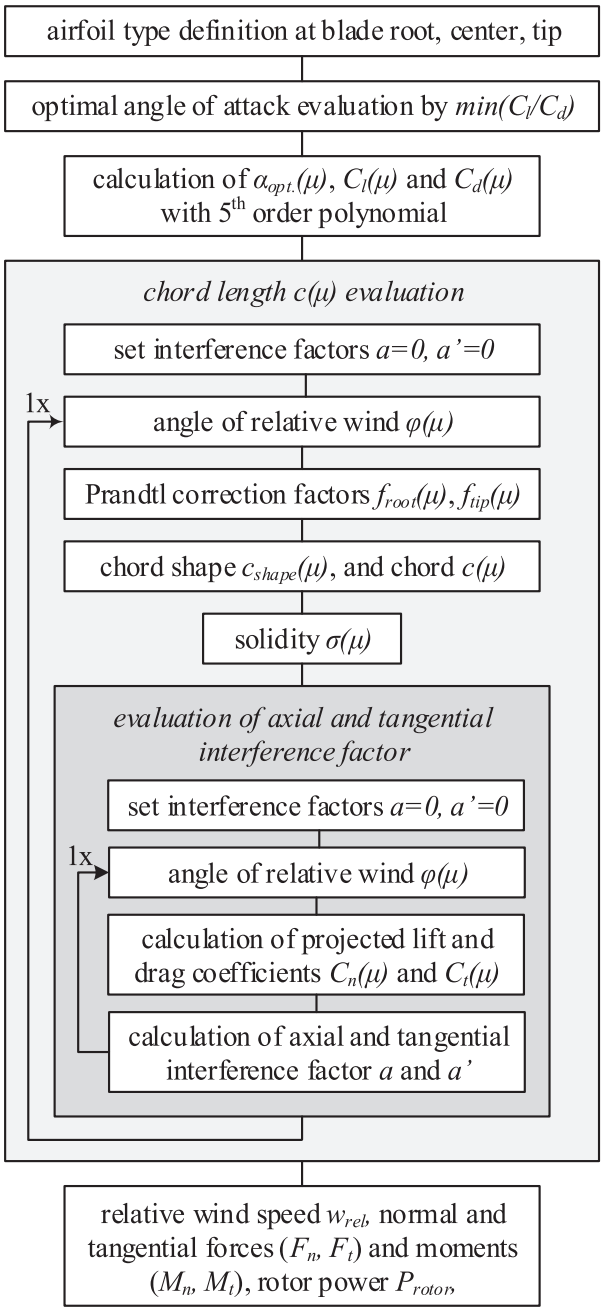

Fig. 3. Blade design calculation procedure at design point.

from the real power. Then, a correction factor may be necessary to adjust the forces, moments and power calculation of the virtual wind turbine rotor. The correction factor can be calculated by comparing the power of the real and virtual wind turbine rotor (cp. also Eq. (16)). As the correction factor is a calculation constant, it can also be added to Eq. (11)–(15). If a correction factor is used, it is crucial to apply it also while calculating the wind turbine loads during operation (cp. section 2.4).

2.3. Effects on wind turbine rotor behavior

In the previous subsections the design procedure of the virtual wind turbine rotor was presented. The virtual rotor was designed based on ideal operation conditions. For example, it was assumed that the wind speed is constant over height and that the blades are not pitched during operation. However, these assumptions are not true while operating the wind turbine. Therefore, in this subsection different effects are presented which influence the behavior of the wind turbine rotor and thus, the rotor loads during operation. In the present paper the effects are limited to wind profile over height, yaw misalignment and side winds, tilt and cone angle as well as tower displacement, individual blade pitching and, wind turbulences. However, other effects, like shear winds, can easily be added to the method. The effects are described analytically in this section. Moreover, their influence on the rotor loads are evaluated separately by a sensitivity analysis in the next section.

The first effect to be considered is the variation of wind speed over height. The wind speed cannot be considered as constant over height because the surface roughness of the landscape around wind turbines, i.e. buildings and trees reduce the wind speed. As the latter is an input parameter for the load calculation (cp. Eqs. (9) and (11) to (15)), it must be evaluated as a function of the surface roughness and height. A logarithmic description of the wind profile as a function of the height H, surface roughness z_o and reference wind speed at a reference height is provided by Ref. [22].

$$v_w(H) = v_{w,ref} \ln\left(\frac{H}{z_o}\right) \Big/ \ln\left(\frac{H_{ref}}{z_o}\right) \tag{20}$$

If both the surface roughness of the area surrounding the considered wind turbine and, for example, the wind speed at the rotor hub height are known, then the wind speed distribution over height can be evaluated and taken into account by the virtual wind turbine rotor. In case a second reference wind speed is available at a second reference height (e.g. at half tower height), the surface roughness need not to be taken from a table like [22] offers, rather, can be calculated from the second reference wind speed. Fig. 4 shows in a simplified manner how the change of the wind speed modifies the direction of the relative wind speed and thus, the magnitude of the relative wind speed and the angle of attack. Consequently, the aerodynamic forces (cp. Fig. 1) vary over height, too. Hence, the wind turbine rotor faces different conditions during one rotor rotation, as it is influenced by the wind speed variation over height.

The second effect to be included is yaw misalignment and the associated side winds. Yaw misalignment occurs if the wind turbine rotor is not exactly aligned to the main direction of wind whereby a side wind hits the wind turbine rotor. Fig. 5 shows, again in a simplified way, the effect of yaw misalignment or side winds. It can be seen that a yaw misalignment is equivalent to side winds in terms of their effect on the wind turbine rotor behavior. From Fig. 5, it is also visible that yaw misalignment and side winds again change the magnitude of the relative wind speed and angle of attack and thus, also the aerodynamic forces. Furthermore, it is

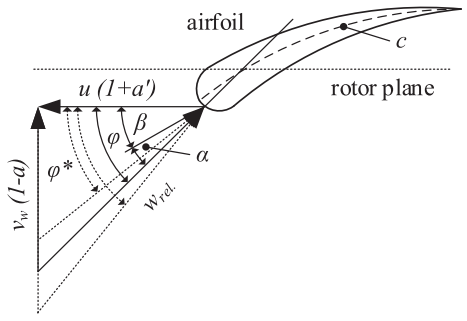

Fig. 4. Changing the wind speed in the wind speed triangle.

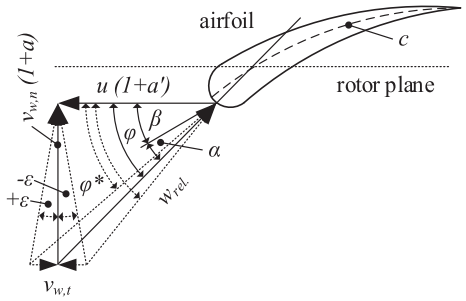

Fig. 5. Effect of side winds and yaw misalignment.

assumed in the present paper that side winds occur purely in horizontal wind direction and that any flow in radial blade direction does not influence the aerodynamic forces and blade behavior. This means that the effects of side winds and yaw misalignment are neglected at horizontal blade positions. Consequently, the changes of the wind speed triangle and aerodynamic forces due to side winds reach their maximum respectively minimum at upper and lower vertical blade position (see also Fig. 6). In addition, based on the yaw misalignment or side wind angle ε (caused by a side wind of magnitude $v_{w,t}$) the modified angle φ^* of relative speed can be described over a rotor rotation (angle ψ) as follows:

$$\tan(\phi^*) = 1 \Big/ \left[\frac{(1+a')}{(1-a)}\mu R\frac{\omega_{rotor}}{v_{w,n}} + \tan(\varepsilon)\sin(\psi)\right] \tag{21}$$

with $\tan(\varepsilon) = \frac{v_{w,t}}{v_{w,n}(1-a)}$.

Note that the side wind angle depends on both side wind direction and rotating direction of wind turbine rotor (clock- or counterclockwise). Therefore, the sign of the side wind angle and thus also the angle of relative speed can change between upper and lower vertical blade position (cp. Fig. 6).

Even though shear winds are not considered in the present paper during the calculation of rotor loads, some considerations will be mentioned at this point. In principle the shear winds can be described in the same way as side winds after Fig. 5 and Eq. (21). In case of shear winds a wind speed component in purely vertical direction (shear wind) must be taken into account instead of a wind speed component in purely horizontal direction (side winds). This means that the angle ε is a shear wind angle instead of a side wind angle and that the effect of shear winds are neglected at vertical blade positions. Then, the changes of the wind speed triangle and aerodynamic forces due to side winds reach their maximum respectively minimum at horizontal blade position. So vertical shear winds have a similar effect as side winds (cp. Fig. 6), but with a 90° shift of the angle ψ.

The third effect to be incorporated in the model is a variation in rotor tilt (γ) angle and blade cone (δ) angle. The modification of the angle of relative wind speed in Eq. (21) includes only the effect of side winds and yaw misalignment. However, wind flow deviations do not only occur because of side winds, but also because of tilt and cone angle as well as tower displacement (cp. Fig. 7). Note that the tilt and cone angle are chosen during wind turbine design to guarantee enough clearance between tower and rotating blades [22]. As shown in Fig. 7 the turbine blades do not rotate anymore in the vertical plane because of the tilt and cone angle as well as tower displacement caused by tower bending. Consequently, it cannot be assumed anymore that the wind flow streams perpendicular to the rotating blade, which is a basic assumption in BEM. Instead, it is assumed that air also flows along the blade in radial direction due to the tilt angle and tower displacement. Then, the air flow respectively wind speed can be decomposed in a modified normal $v_{w,n'}$ and radial $v_{w,r'}$ wind speed (cp. Fig. 7). The Cartesian coordinates now refer to the blade axis instead of the vertical plane, i.e. *rtn*-coordinates change to *r't'n'*-coordinates by rotating around the *t*-axis (cp. Fig. 8) with the angle χ (see Eq. (23)). Using the modified, normal wind speed (*r't'n'*-coordinates) for the calculation of the aerodynamic forces means that both lift and drag forces as well as blade resulting forces are rotated by the tilt angle. Fig. 8 shows the wind speed triangle due to a combination of side wind, tilt and cone angle as well as the resulting aerodynamic forces. It can be seen that the reacting forces at the blades are not any longer just in the vertical plane or perpendicular to it, but an additional force is generated in the radial direction of the rotor plane (cp. Fig. 8 – aerodynamic forces). By comparing Figs. 1 and 8 one can see that the tilt and cone angle as well as tower displacement must also be considered in Eq. (7a) and (7b) and Eqs. (14) and (15). Furthermore, it is visible in Fig. 7 that the blade – vertical plane angle and tower displacement changes over one rotor rotation. The projected lift and drag coefficients normal, tangential and radial to the rotor plane are then defined as follows:

$$C_n = [C_l\cos(\phi) + C_d\sin(\phi)]\cos(\chi) \tag{22a}$$

$$C_t = [C_l\sin(\phi) - C_d\cos(\phi)]\cos(\chi) \tag{22b}$$

$$C_r = [C_l + C_d]\sin(\chi) \tag{22c}$$

with the blade vertical plane angle

$$\chi = \delta - (\gamma_{tilt} + \gamma_{tower})\sin(\psi) \tag{23}$$

Note that $\psi = 0$ at the horizontal blade position and $\pi/2$ at the top position.

Moreover, due to the radial blade force (cp. Fig. 8 – aerodynamic forces) and the tilted respectively coned blade, an additional radial

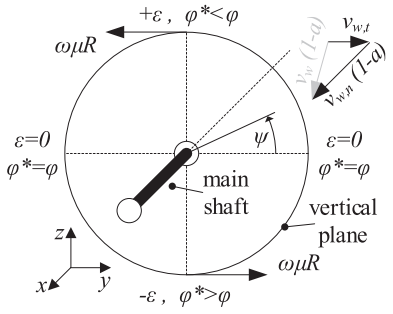

Fig. 6. Modified relative wind angle due to side wind.

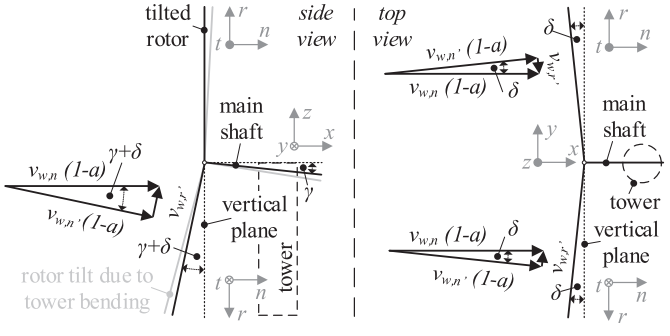

Fig. 7. Rotor side and top view due to tilt (γ) and cone (δ) angle as well as tower displacement for $\gamma = \delta$

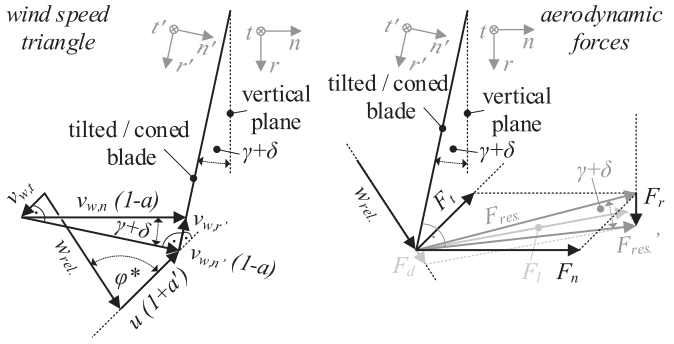

Fig. 8. Wind speed triangle and aerodynamic forces due to tilt angle at lower blade position.

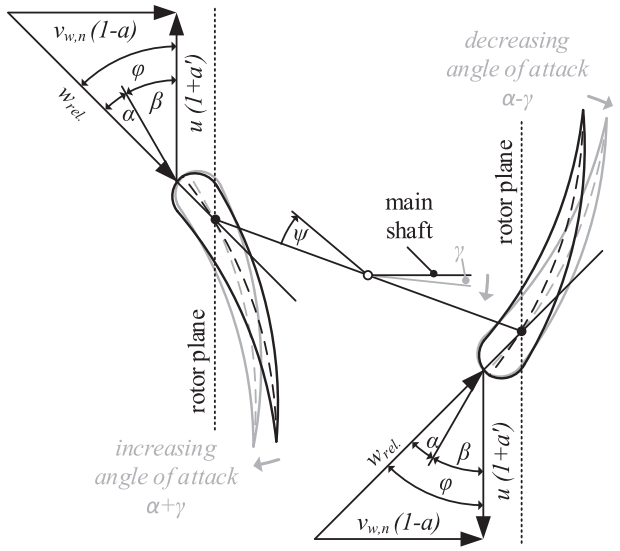

Fig. 9. Changing angle of attack due to tilt angle.

blade force and blade bending moment are generated which complement Eq. (11)–(15). On the basis of Eq. (22a-c), blade bending moments are specified around the tangential direction of the rotor plane as:

Radial blade force (per unit blade length)

$$F_r^m = \frac{\rho}{2} w_{rel.}^2 c C_r \tag{24}$$

Total blade radial force

$$F_r = R \int_{\mu_{root}}^{1} F_r^m d\mu \tag{25}$$

Blade bending moments around tangential axis

$$M_{t,1} = R^2 \cos(\chi) \int_{\mu_{root}}^{1} F_n^m \mu d\mu \tag{26}$$

$$M_{t,2} = R^2 \sin(\chi) \int_{\mu_{root}}^{1} F_r^m \mu d\mu \tag{27}$$

In addition, it is important to note that the tilt angle and tower displacement do not only affect the wind inflow at the leading edge of the airfoils or blade, but also the wind inflow angle, i.e. angle of attack, at horizontal blade positions (cp. Fig. 9). In other words, tilt angle and tower displacement cause blade pitching in horizontal blade position. This means that the blades are positively and negatively pitched during one rotor rotation. Consequently, the angle of attack changes and thus, the aerodynamic force, too, because the angle of attack directly influences lift and drag values of the airfoils. Note also that the blade cone angle does not influence the angle of attack over one rotor rotation. Fig. 9 shows, furthermore, that the change of angle of attack at a tilted rotor is equal to the tilt angle or tower displacement. Hence, the fluctuating angle of attack due to tilt angle and tower displacement can be described over one rotor rotation by:

$$\Delta\alpha_{tilt} = [\gamma_{tilt} + \gamma_{tower}]\cos(\psi) \tag{28}$$

Tilt and cone angle as well as tower displacement finally also influence the blade mass forces because the blades do not rotate exactly in the vertical plane. This means that blade mass forces also occur in the direction normal to the vertical plan. If the blade is not pitched during operation, i.e. the blade does not move, then the acceleration of the blade mass due to regular rotation is specified by Ref. [23] as: $\vec{a} = -\vec{\omega} \times (\vec{\omega} \times \vec{r})$. The blade accelerations are then calculated by considering the angular main shaft speed ω_0 and circular path of the blade center of gravity (*cog*) over one rotation.

$$\vec{\omega} = \omega_0 \begin{pmatrix} \cos(\gamma) \\ 0 \\ -\sin(\gamma) \end{pmatrix}_{xyz} \tag{29}$$

$$\vec{r}(t) = R_{cog} \begin{pmatrix} -\sin(\chi) \\ \cos(\chi)\cos(\omega t) \\ \cos(\chi)\sin(\omega t) \end{pmatrix}_{xyz} \tag{30}$$

Whereas all previous equations have been defined in the (individual) blade coordinate system *rtn*, the description of the complete rotor now requires to shift to a more global rotor coordinate system. Thus, both angular main shaft speed and circular path are expressed here in *xyz*- coordinates. The *xyz*-coordinates are inertial (Cartesian) coordinates whose origin is placed in the vertical plane and at the hub center (see Fig. 10). For evaluating the position vector in Eq. (30), the radius of the blade center of gravity is required. After Grote and Antonsson [23] the center of gravity is calculated by $R_{cog} = \int_0^R r\rho dV / \int_0^R \rho dV$. To simplify the calculation of the center of gravity, it is assumed here that the blade mass is homogeneously distributed and that the blade surface is proportional to the blade volume. Hence, the center of gravity can be approximated as:

$$R_{cog} = \frac{\int_0^R r dA}{\int_0^R dA} = R \frac{\sum_i (\mu_i \Delta\mu_i c_i)}{\sum_i (\Delta\mu_i c_i)} \tag{31}$$

Then, based on Eqs. (29) and (30) the acceleration of the blade mass due to rotation around the main shaft axis is defined as:

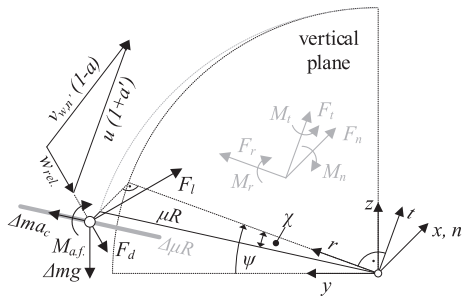

Fig. 10. Overview of loads acting on a of blade element.

$$\vec{a}_{c,xyz}(t) = R_{cog}\omega_0^2 \begin{pmatrix} \sin^2(\gamma)\sin(\chi) - \frac{1}{2}\sin(2\gamma)\cos(\chi)\sin(\omega t) \\ \cos(\chi)\left[\sin^2(\gamma)\sin(\omega t) + \cos^2(\gamma)\cos(\omega t)\right] \\ \cos^2(\gamma)\cos(\chi)\sin(\omega t) - \frac{1}{2}\sin(2\gamma)\sin(\chi) \end{pmatrix}_{xyz} \tag{32}$$

In the same way the gravitational acceleration can also be described in *xyz* coordinates.

$$\vec{g} = \begin{pmatrix} 0 \\ 0 \\ -g_0 \end{pmatrix}_{xyz} \tag{33}$$

Thus, the total blade mass force, which acts on the blade in addition to aerodynamic forces and moments, is given in *xyz*-coordinates as: $\vec{F}_{m,bl} = m_{bl}[\vec{a}_c(t) + \vec{g}]_{xyz}$.

The fourth effect to be included is the blade pitching effect. As already mentioned, the tilt angle pitches the blades in horizontal blade position (cp. Eq. (28)). Blade pitching, however, is also done actively by individual blade pitch control units. This means that every blade of the wind turbine rotor can operate with an individual angle of attack. Consequently, the aerodynamic forces differ from blade to blade which makes that the aerodynamic rotor unbalance increases. The change in angle of attack α is directly linked to the individual pitch control (pitch angle β) and does not depend on the rotor position:

$$\Delta\alpha(\psi) = \Delta\beta(\psi) \tag{34}$$

The fifth and final effect to be included is wind turbulence, which also affects the aerodynamic blade forces and thus, the wind turbine rotor behavior. Wind turbulences are wind speed fluctuations. Therefore, a simplified description, which is usable for the BEM theory, is the variation of wind speed v_w along the blade radius and over one rotor rotation. So wind turbulences are similarly specified as the change of wind speed over height (cp. also Fig. 4). By introducing a wind speed correction factor, a simplified analytical description is provided for wind turbulences.

$$\begin{aligned} v_{w,turb}(\mu,\psi) &= k_{turb}(\mu,\psi)^* v_w \\ k_{turb}(\mu,\psi) &= 1 + A\sin(2i\pi\mu)\sin(j\psi) \end{aligned} \tag{35}$$

Thereby, the amplitude A defines the magnitude of the wind speed fluctuation, i the number of wind speed fluctuations along the blade radius and j the number of wind speed fluctuations over one rotor rotation. Note that Eq. (35) is a very simplified way to describe wind turbulences. Consequently, any calculation results based on Eq. (35) must be interpreted carefully. However, this expression does enable to check the sensitivity of blade loads on turbulence level, as it will be shown in section 3.

2.4. Calculation procedure for blade forces and moments during operation

In the previous two subsections the design procedure of the virtual wind turbine rotor and blades as well as the different effects on the wind turbine rotor behavior were introduced. The design of the virtual blade was described for one specific operating point (blade design point) under ideal conditions excluding any effects during operation. However, for evaluating the wind turbine rotor loads during operation it is necessary to follow a calculation procedure which considers the different effects (as discussed in section 2.3). This means that the calculation procedure of Fig. 3 must be modified. It is important to note that due to these effects the angle of attack and relative speed change continuously over one rotor rotation. This means that the axial and tangential interference factor must be re-calculated for every blade position and operating condition. Fig. 11 shows the modified calculation procedure which is used for determining the loads of the wind turbine rotor. As now the aerodynamic blade loads are calculated, the torsional blade moment generated by the airflow around the airfoil [24] is included in Fig. 11. Note that this blade pitching moment was not considered in the design of the virtual blade and wind turbine rotor (cp. Fig. 3).

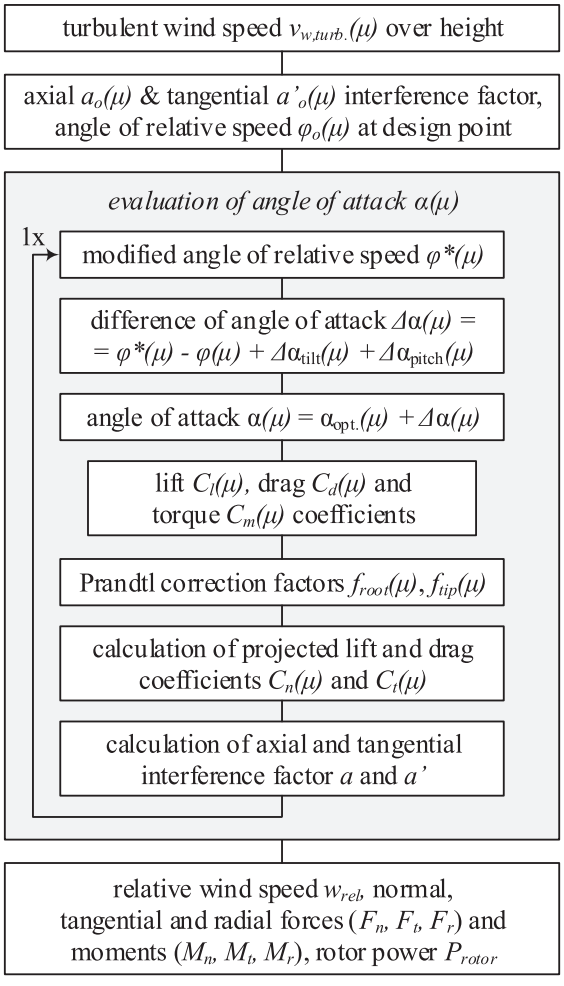

Fig. 11. Calculation procedure of aerodynamic blade loads.

For the aerodynamic load calculation, it is assumed in the present paper that the blade is rigid i.e. the blade does not deform due to torsional and bending moments. This assumption is not true in reality; however, it provides the advantage that the change of angle of attack and relative wind due to blade deformations can be neglected during the load calculation of the blade and wind turbine rotor.

Further, one can see by comparing Figs. 3 and 11 that the purpose of the calculation procedure in Fig. 3 is the evaluation of the chord shape (blade geometry) and axial and tangential interference factors at the blade design point. In contrary, the purpose of the calculation procedure in Fig. 11 is the calculation of the angle of attack during operation including the different effects described in the previous subsection. Based on the angle of attack, which is continuously calculated, the lift, drag and torque coefficients are evaluated and thus, also the resulting forces and moments during operation. By following the calculation procedure in Fig. 11 the normal, tangential and radial forces and moments are calculated along the blades i.e. for the different blade sections (elements) needed to apply the BEM theory. To illustrate this, Fig. 10 schematically shows the centrifugal, gravity and aerodynamic forces as well as the pitching moment acting on a blade element with a length $\Delta\mu R$ at a radius μR. The blade element forces and moments are described and calculated in the rotating rtn-coordinates. The rtn-coordinates have the same origin as the xyz coordinates; however, the rtn coordinates rotate over the angle $\psi = \omega t$ (cp. also Fig. 10). Hence, the blade root forces and moments (in rtn-coordinates) are the sum of all forces and moments of the different elements. The blade root force and moment written as time dependent vectors are specified as follows:

$$\vec{F}_{bl}(t) = m_{bl}\left[\vec{a}_c - g_0\begin{pmatrix}\sin(\omega t)\\ \cos(\omega t)\\ 0\end{pmatrix}\right]_{rtn} + \begin{pmatrix}\sum_i (F_r(\mu_i))\\ \sum_i (F_t(\mu_i))\\ \sum_i (F_n(\mu_i))\end{pmatrix}_{rtn} \tag{36}$$

$$\vec{M}_{bl} = R_{cog}\begin{pmatrix}\cos(\chi)\\ 0\\ -\sin(\chi)\end{pmatrix}_{rtn} \times m_{bl}\left[\vec{a}_c - g_0\begin{pmatrix}\sin(\omega t)\\ \cos(\omega t)\\ 0\end{pmatrix}\right]_{rtn} + R_{bl}\begin{pmatrix}\cos(\chi)\\ 0\\ -\sin(\chi)\end{pmatrix}_{rtn} \times \begin{pmatrix}\sum_i (\mu F_r(\mu_i))\\ \sum_i (\mu F_t(\mu_i))\\ \sum_i (\mu F_n(\mu_i))\end{pmatrix}_{rtn} - \sum_i \left(M_{a.f.}(\mu_i)\right)_{rtn}\begin{pmatrix}\cos(\chi)\\ 0\\ -\sin(\chi)\end{pmatrix}_{rtn} \tag{37}$$

with $F_r(\mu) = F_{aero}(\mu)\cdot C_r(\mu)$, $F_t(\mu) = F_{aero}(\mu)\cdot C_t(\mu)$, $F_n(\mu) = F_{aero}(\mu)\cdot C_n(\mu)$, $F_{aero}(\mu) = \frac{\rho}{2}\cdot w_{rel.}^2(\mu)\cdot c(\mu)$, $M_{a.f.}(\mu) = F_{aero}(\mu)\cdot c(\mu)\cdot C_m(\mu)$ and $a_{c,rtn}(t) = \begin{pmatrix}0 & 0 & 1\\ \cos(\omega t) & -\sin(\omega t) & 0\\ \sin(\omega t) & \cos(\omega t) & 0\end{pmatrix}^{-1} a_{c,xyz}(t)$.

The blade root force and moment (loads) are calculated for every blade and rotor rotating angle ψ (or time instance t). Then, the blade root loads are transformed from the rotating *rtn*-coordinates to initial *xyz*-coordinates. The resulting loads of all (three) blades, i.e. the sum of blade root loads of all blades, constitute the loads of the wind turbine rotor hub. Note that to simplify the calculation algorithms the mass forces of the entire blade are reduced in the present paper to a point force i.e. only aerodynamic forces are considered here as distributed forces.

In summary, based on the calculation procedure shown in Fig. 11 and based on Eqs. (36) and (37), forces and moments (loads) of the virtual blades respectively virtual wind turbine rotor can be quantified for different operating conditions, as it will be demonstrated in the section 3.

2.5. Limitations of the analytical rotor model

After introducing the calculation procedure for blade and wind turbine rotor loads, some limitations of this calculation procedures will be mentioned in this subsection. First, the BEM theory is an approximation of the real blade design implying that the load calculation results may deviate from the real loads. A correction factor was introduced to overcome this problem. Second, the effects demonstrated in section 2.3 are based on assumptions and simplifications while describing the wind speed triangle and its angles during different operating conditions. The accuracy of the calculation results may be reduced by these assumptions and simplifications. Third, the angle of relative speed (cp. Eq. (21)), axial and tangential interference factor, angle of attack as well as lift and drag coefficients are not independent (cp. Fig. 11). If the change of angle of attack is so high that values of the projected lift and drag coefficient (cp. Eq. (22a) to (22c)) change their sign, then the normal calculation of the interference factors (cp. Eq. (1a) and (1b) and Eq. (2)) and relative angle of wind (cp. Eq. (21)) will fail. On the other hand, it can be argued that a wind turbine should not run under conditions where the projected lift and drag values change their sign because this means that either the lift coefficient is negative or the drag coefficient is very high. A negative lift coefficient turns the direction of the lift force by 180° and a high drag coefficient is equivalent to a huge blade thrust force. So it can be assumed that the set of equations used for the calculation procedure shown in Fig. 11 do not fail during regular operation. Nevertheless, it is important to monitor the values of the interference factors during the analyses in order to detect load calculation failures.

3. Load calculations

In this section the load calculation as described by Fig. 11, Eqs. (36) and (37) is applied to a three bladed upwind wind turbine rotor which is designed based on the values of Tables 1–3 (cp. also section 2.2). The virtual model of this wind turbine rotor is used for performing load sensitivity analyses in order to evaluate the influence of wind profile over height, yaw misalignment and side winds, tilt and cone angle, tower displacement, individual blade pitching and wind turbulences (cp. section 2.3). The loads are analyzed at three locations: at the blade root, the hub center of the wind turbine rotor as well as the tower head. All calculations are executed with an average wind speed of 8.5 m/s at a hub height of 94 m. An agricultural terrain is assumed with very few buildings and trees, i.e. the surface roughness factor is set equal to 0.03 (cp. also [22]). Furthermore, different scenarios are considered for the sensitivity analyses in order to demonstrate the different effects on the wind rotor behavior. Tables 4 and 5 show the parameter settings of the different scenarios which take into account wind speed over height (h), negative and positive yaw misalignment (y), negative and positive pitching (p) of one blade and turbulences

Table 4
Different scenarios for load calculations with a tilt and cone angle of 0°.

Scenario	Surface roughness	Yaw angle ε	Pitch angle β	Tilt/cone angle γ/δ	Turbu-lences
h-t0°	0.03	0°	0°	0°	no
y -0.1°	0.03	−0.1°	0°	0°	no
y + 0.1°	0.03	+0.1°	0°	0°	no
p -0.1°	0.03	0°	−0.1°	0°	no
p + 0.1°	0.03	0°	+0.1°	0°	no
turb. 2%	0.03	0°	0°	0°	±1%

Table 5
Different scenarios for load calculations with a tilt and cone angle of 6°.

Scenario	Surface roughness	Yaw angle ε	Pitch angle β	Tilt/cone angle γ/δ	Turbu-lences
h-t6°	0.03	0°	0°	6°	no
y -3°	0.03	-3°	0°	6°	no
y + 3°	0.03	+3°	0°	6°	no
p -1.5°	0.03	0°	−1.5°	6°	no
p + 1.5°	0.03	0°	+1.5°	6°	no
turb. 5%	0.03	0°	0°	6°	±2.5%

(*turb.*). The parameters of the turbulence (Eq. (35)) are set to: $i = 33, j = 720, A = 0.01$ (scenario *turb. 2%*) respectively $A = 0.025$ (*turb. 5%*). Moreover, the rotor tilt (t) and blade cone angles are set equally, i.e. $\gamma = \delta$. This means that the blades are in the vertical plane at the upper position (cp. Figs. 7 and 10). In addition, the load sensitivity analyses are performed using equivalent loads which are calculated from the evaluated forces, moments and dimensions like radii or shaft lengths. These equivalent loads neglect the masses of the hub, main shaft, gearbox and direct drive generator because mass gravity forces act only in vertical (or radial) direction, while the dominant power train loads act in axial and circumferential direction. Further, the gravity forces only act as a load offset, i.e. they do not influence the load fluctuations and dynamic loads. The drawback of neglecting the mass gravity forces of the different drive train components is that the calculated equivalent loads may be lower than the real loads. The advantage, however, is that the results presented in this section are generic, and thus valid for any wind turbine independent of its drive train concept.

3.1. Loads at blade root

The forces and moments acting at the blade root must not only be carried by the blade itself but also by the pitch bearing. Therefore, the load sensitivity analysis at the blade root is performed by evaluating equivalent pitch bearing loads. Fig. 12 schematically shows the assembly of a turbine blade, pitch bearing and rotor hub. Then, the equivalent pitch bearing load can be specified based on Fig. 12 in the rotating coordinate frame *r't'n'*. Note that the *r'*-axis is aligned with the blade longitudinal axis and that the *r't'n'*-coordinates are obtained by rotating the *rtn*-coordinates by the blade rotor plane angle χ around the t-axis (cp. also Fig. 10).

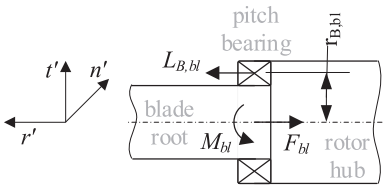

Fig. 12. Loads of blade root at the pitch bearing.

$$\vec{L}_{B,bl} = \vec{F}_{bl} + \frac{\vec{M}_{bl}}{|\vec{r}_{B,bl}|^2} \times \vec{r}_{B,bl} = \begin{pmatrix} F_{bl,r'} \\ F_{bl,t'} \\ F_{bl,n'} \end{pmatrix} + \begin{pmatrix} M_{bl,r'} \\ M_{bl,t'} \\ M_{bl,n'} \end{pmatrix} \times \begin{pmatrix} 0 \\ 1/r_{B,bl} \\ 1/r_{B,bl} \end{pmatrix} \tag{38}$$

The equivalent pitch bearing load as defined in Eq. (38) is evaluated for the different scenarios shown in Tables 4 and 5. To compare the different parameter settings, the absolute values of the equivalent blade root loads are calculated with blade root/bearing radius $r_{B,bl} = 1.15m$. Figs. 13 and 14 show the results for the different scenarios. It is noteworthy that pitch angle deviation of one blade, yaw misalignment or fluctuations of the lift and drag forces (turbulences) have only a minor influence on the equivalent blade root loads. An effect that cannot be neglected is caused by a variation of tilt and cone angle. One can see by comparing Figs. 13 and 14 that the magnitude of the dynamic load, i.e. the load fluctuation over one rotor rotation is increased by increasing simultaneously both the tilt and cone angle. However, the most dominant load variation observed in these figures is governed by the rotation angle. Equations (36) and (37) show that the mass forces are responsible for this variation.

The different accelerations acting on the blade mass need to be considered in more details. Until now, a rigid blade was assumed which was also not pitched during operation. But blade flapping

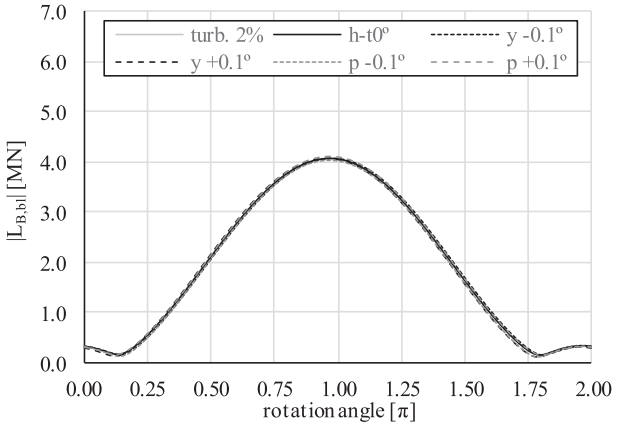

Fig. 13. Absolute value of pitch bearing load for the scenarios in Table 4.

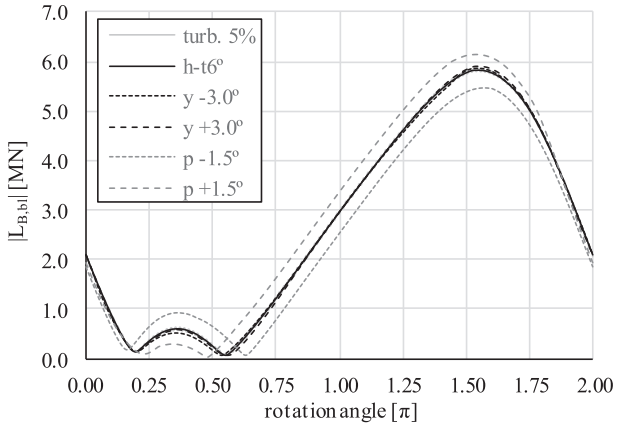

Fig. 14. Absolute value of pitch bearing load for the scenarios in Table 5.

and pitching cause additional accelerations of the blade mass because the blade rotates. Consequently, Euler and Coriolis forces also act on the blade mass. After [23] the Euler acceleration is defined as $\vec{a}_{Euler} = \vec{\omega} \times \vec{r}_{cog}$ and the Coriolis acceleration as $\vec{a}_{Coriolis} = 2\vec{\omega} \times \vec{v}_{cog}$ where $\vec{r}_{cog}$ and $\vec{v}_{cog}$ are the radial position and velocity of the blade center of gravity respectively. For evaluating the influence of Euler and Coriolis acceleration on the blade root loads, the magnitude of the Euler, Coriolis, centrifugal acceleration and gravity are compared. To do so, the blade pitch and cone angles including the effect of blade pitching and flapping are described as follows:

$$\Delta\beta(t) = \beta_0 + \Delta\alpha_h \sin(\omega t) \tag{39}$$

$$\delta(t) = \delta_0 + \Delta\delta \sin(k\omega t) \tag{40}$$

Equation (39) assumes that pitching is used for the change of angle of attack needed to compensate the effect of wind speed over height. Other effects that cause a change of the angle of attack over one rotor rotation are not considered here because Eqs. (39) and (40) are only used to demonstrate the influence of Euler and Coriolis acceleration. In reality, Eq. (39) is dictated by the pitch control system and Eq. (40) could be derived from measurements of blade flapping. The factor k indicates the number of blade flaps per rotor rotation. The angle δ_0 is defined by the blade coning and the angle difference $\Delta\delta$ is the cone angle fluctuation due to blade flapping. Based on Eqs. (39) and (40) the radius and velocity of the blade mass center as well as angular velocity and acceleration are specified in *rtn*-coordinates for a tilt angle $\gamma = 0$ as.

$$\vec{r}(t) = R_{cog} \begin{pmatrix} \cos(\delta(t)) \\ -\sin(\delta(t))\sin(\beta + \Delta\beta_p(t)) \\ -\sin(\delta(t))\cos(\beta + \Delta\beta_p(t)) \end{pmatrix}_{rtn} \tag{41}$$

$$\vec{v}_{cog}(t) = = -\omega_0 R_{cog} \begin{pmatrix} k\Delta\delta \sin(\delta(t))\cos(k\omega_0 t) \\ k\Delta\delta\cos(\delta(t))\cos(k\omega_0 t)\sin(\beta+\Delta\beta_p(t)) \\ k\Delta\delta\cos(\delta(t))\cos(k\omega_0 t)\cos(\beta+\Delta\beta_p(t)) \end{pmatrix}_{rtn} + \omega_0 R_{cog} \begin{pmatrix} 0 \\ -\Delta\alpha_h \sin(\delta(t))\cos(\beta+\Delta\beta_p(t))\cos(\omega_0 t) \\ \Delta\alpha_h \sin(\delta(t))\sin(\beta+\Delta\beta_p(t))\cos(\omega_0 t) \end{pmatrix}_{rtn} \tag{42}$$

$$\vec{\omega}(t) = \omega_0 \begin{pmatrix} \Delta\alpha_h \cos(\omega_0 t) \\ 0 \\ 1 \end{pmatrix}_{rtn} \tag{43}$$

$$\dot{\vec{\omega}}(t) = \omega_0^2 \begin{pmatrix} -\Delta\alpha_h \sin(\omega_0 t) \\ 0 \\ 0 \end{pmatrix}_{rtn} \tag{44}$$

The centrifugal, Euler and Coriolis accelerations acting at the blade mass center (cp. Fig. 15) are calculated based on Eq. (41)–(44). Furthermore, for detecting the influence of Euler and Coriolis acceleration on the blade root loads the following calculation parameters are assumed: blade cone angle $\delta_0 = 10°$, cone angle fluctuation $\Delta\delta = 2°$, number of blade flaps (wind gusts) per rotor rotation $k = 12$, blade pitch angle $\beta_0 = 0$ and correction of angle of attack by blade pitching $\Delta\alpha_h = 6°$ (cp. also Eq. (34)). The angular velocity of the main shaft is considered here as constant. In reality an unsteady angular shaft velocity would additionally cause Euler and Coriolis accelerations. In Fig. 16 the absolute values of Euler, Coriolis, centrifugal and gravity accelerations are plotted over one rotor rotation. It can be seen that the ratio between gravity and Euler acceleration and between centrifugal and Coriolis acceleration is approximately ten. Therefore, both Euler and Coriolis acceleration and their associated forces cannot be neglected because, for example, the ball bearing life time is proportional to bearing loads by the power three [25]. A load increase due to Euler and Coriolis acceleration by approx. 10% leads thus to a bearing life time reduction of approx. 25%. In addition, one can see in Fig. 16 that the Coriolis acceleration caused by blade flapping can fluctuate with a much higher frequency than the main shaft rotation frequency. This means that the Coriolis acceleration causes high-cycle loads and

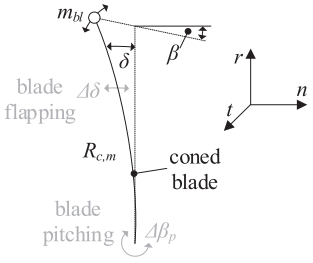

Fig. 15. Pitching and flapping of coned blade.

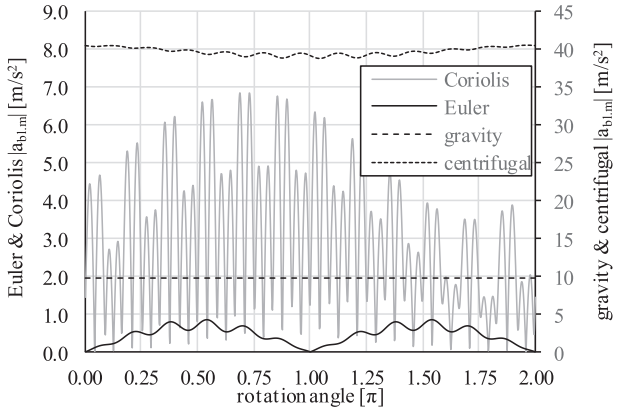

Fig. 16. Absolute value of blade mass accelerations.

thus, contributes to the high-cycle fatigue of the blade and pitch bearing. For extending the life time of blade and pitch bearing the magnitude of Euler and Coriolis accelerations should be reduced to a minimum during operation. The minimization of Euler and Coriolis accelerations can only be achieved by smoothing unsteady behavior of angular shaft speed and blade pitching. However, blade flapping always occurs and even though the angular acceleration is assumed equal to zero, Coriolis acceleration still has a significant influence on the blade root load profiles and thus, the life time of the blade and pitch bearing.

3.2. Loads at rotor hub

In the previous subsection loads at the blade root were evaluated. Now, loads at the rotor hub center are analyzed and are derived from the blade root loads because hub center loads are equal to the sum of all blade root loads. This means that some blade root loads negate each other and some are additive. Furthermore, the resultant hub center loads must be absorbed by main bearings (cp. Fig. 17). So analogous to the blade and pitch bearing loads, the main bearing loads are equivalent to the hub center loads. As the mass gravity forces of the different components connected to the main shaft are neglected in the present paper, the main bearing loads can be used as an equivalent hub center load for the load sensitivity analysis. Without considering the mass gravity forces, the loads on the two bearings (L_{B1} and L_{B2}) are described in $x'y'z'$-coordinates as follows:

$$\vec{L}_{B1} = \vec{l}_{HB}\vec{F}_{hub} + \frac{1}{l_B}\vec{M}_{hub,b} = \begin{pmatrix} 1 \\ 1+\frac{l_H}{l_B} \\ 1+\frac{l_H}{l_B} \end{pmatrix}^T \begin{pmatrix} F_{hub,x'} \\ F_{hub,y'} \\ F_{hub,z'} \end{pmatrix} + \frac{1}{l_B}\begin{pmatrix} 0 \\ M_{hub,y'} \\ M_{hub,z'} \end{pmatrix} \quad (45)$$

$$\vec{L}_{B2} = -\left[\vec{l}_H\vec{F}_{hub} + \frac{1}{l_B}\vec{M}_{hub,b}\right] = -\begin{pmatrix} 0 \\ \frac{l_H}{l_B} \\ \frac{l_H}{l_B} \end{pmatrix}^T \begin{pmatrix} 0 \\ F_{hub,y'} \\ F_{hub,z'} \end{pmatrix} + \frac{1}{l_B}\begin{pmatrix} 0 \\ M_{hub,y'} \\ M_{hub,z'} \end{pmatrix} \quad (46)$$

The $x'y'z'$-coordinates are obtained by rotating the xyz-coordinates over the tilt angle γ around the y-axis. In addition, it is assumed here that the bearing *B1* absorbs both axial and radial forces and, bearing *B2* only radial forces.

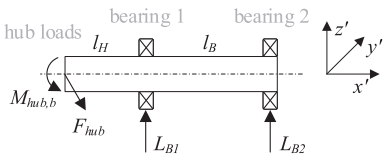

Fig. 17. Loads of rotor hub and main bearings.

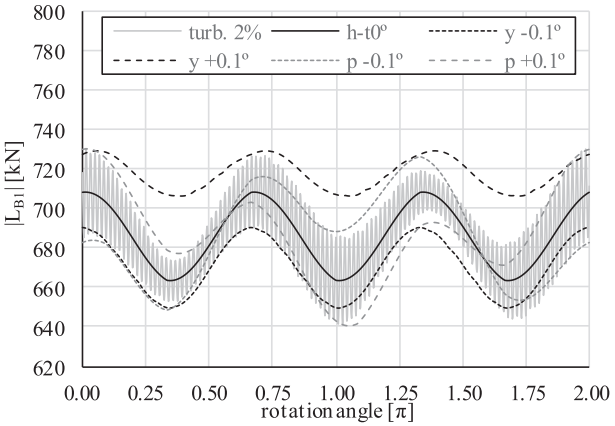

Fig. 18. Absolute value of main bearing load (B1) for the scenarios in Table 4.

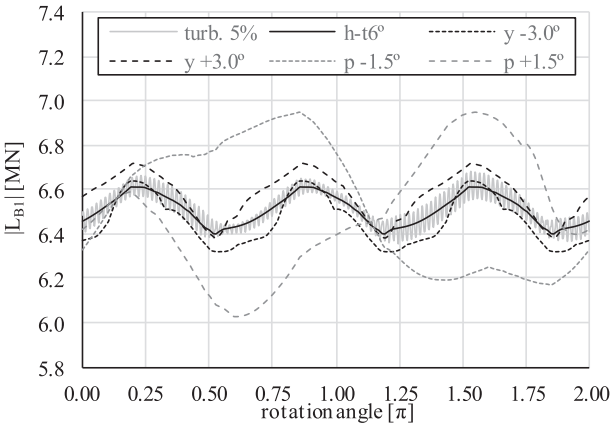

Fig. 19. Absolute value of main bearing load (B1) for the scenarios in Table 5.

To compare again the different scenarios of Tables 4 and 5, the equivalent load of the main bearing B1 is evaluated using Eq. (45) with shaft distances $l_B = 1.0m$ and $l_H = 0.75m$. Figs. 18 and 19 show the absolute values of the equivalent loads on B1 for the different scenarios. First, one can see that the change of both tilt and cone angle from 0° to 6° (Fig. 18 versus 19) increases the bearing loads (L_{B1}) by a factor of almost ten. Note that at the hub center the blade bending moments due to gravity are balanced out at a purely tilted rotor and are summed up at a purely coned rotor. This means that the bearing load increase is mainly caused by the cone angle. It is also important to remember that the tilt and cone angles are chosen while designing the wind turbine. Second, depending on the side wind direction (or yaw misalignment) a negative or positive offset is observed in the bearing loads. So side winds or yaw misalignment can either decreases or increases the average loads (and life time) of the main bearings. Third, individual blade pitching increases the dynamic part (fluctuating load amplitude) of the main bearing loads independent of negative or positive pitch angle. Consequently, the bearing peak loads also increase due to individual pitching (cp. Fig. 19 *p-1.5°*/*p+1.5°* vs. *h-t6°*). Fourth, it is visible that the frequency of the main bearing loads (L_{B1}) variation, i.e. three cycles over a 2π rotation angle, equals the product of the main shaft frequency and number of blades. The origin of this relation is the wind speed difference over height causing the aerodynamic blade loads to vary over one rotor rotation (cp. also [26]). However, in Figs. 18 and 19 it can also be observed that due to blade pitching the bearing load frequency shifts from

Table 6
Equivalent load and main bearing life time for $v_{wind} = 8$ m/s.

Parameter setting	Equivalent load $L_{eq.}$	Bearing life time $(1/L_{eq.})^3$	Δ life time [%]
h-t6°	1.000	1.000	0.00
y -3.0°	1.027	0.924	−7.56
y + 3.0°	0.984	1.050	5.01
p -1.5°	1.016	0.953	−4.73
p + 1.5°	0.992	1.026	2.58
turb. 5%	1.001	0.997	−0.31

the third to the first rotor harmonic depending on the magnitude of the pitch angle variation. The shift from the third to the first harmonic is provoked by pitch angle deviation (or individual blade pitching). If one blade is pitched individually, its angle of attack and associated aerodynamic forces differ from the other two blades. Consequently, the aerodynamic imbalance (peak load) increases and becomes dominant over the initial (3rd harmonic) load variation due to wind speed fluctuation. Fifth, load fluctuations due to wind turbulences are also visible in the bearing loads (cp. Figs. 18 and 19) and they increase both the peak-to-peak loads and the frequency. Therefore, wind turbulences negatively influence the life time of the main bearings.

In order to quantify the influence of yaw misalignment, pitch angle deviation and turbulences on the bearing loads (and life time), ball bearing loads are evaluated over one rotor rotation. Equivalent loads are calculated for constant shaft speeds using [27].

$$L_{B1,eq.} = \sqrt[3]{\sum_i \left(q_i \cdot L_{B1,i}^3\right)} \tag{47}$$

Equation (47) expresses that the combination of i different loads, each with a relative occurrence q_i (in time or revolutions), leads to an equivalent load $L_{B1,eq.}$. The equivalent bearing load is calculated for one rotor rotation using $i = 720$ and for each of the six plotted curves shown in Fig. 19 (and presented in Table 6). For comparing them, curve *h-t6°* is used as reference because the curve *h-t6°* only includes the effect of tilt and cone angle and wind speed over height. The relative bearing life time L_{10} is also shown, assuming that it is proportional to $1/L_{eq.}^3$ [25]. Moreover, centrifugal and aerodynamic forces, as well as aerodynamic moments, are proportional to the square of the wind speed (eq. (11)–(15) and eqs. (32) and (36)). So the life time is proportional to the 6th power of the wind speed.

$$L_{10} \sim \left(1/L_{eq.}\right)^3 \sim \left(1/v_w^2\right)^3 \sim 1/v_w^6$$

Table 6 demonstrates that the equivalent bearing loads are affected by both negative and positive yaw misalignment and pitch angle deviations. This means that the bearing life time is extended or reduced depending on negative or positive yaw misalignment and pitch angle deviation. Table 6 shows additionally that load fluctuations due to wind turbulences reduce the bearing life time, too, but the magnitude of the effect is much smaller.

From a first point of view it seems that yaw misalignment, pitch angle deviation and wind turbulences may have minor influences on the main bearing loads (approx. 1-3%). However, it is important to note that these effects can occur simultaneously. Moreover, this demonstration calculation neglected (actively controlled) blade pitching and flapping. Further, the calculations were performed at a wind speed of 8.5 m/s, with a wind speed fluctuation of ±2.5% and a constant angular shaft speed. However, as was shown before the bearing life time is proportional to the power six of the wind speed (for wind speeds < rated wind speed). Therefore, the negative and positive life time differences calculated in Table 6 change with increasing wind speed. Table 7, with the results for a wind speed of 12 m/s, confirms that the wind speed distribution over time has a dominant effect on the main bearing life time but now also with a magnitude that cannot be neglected.

Summarizing the load calculation at the rotor hub center or rather at the main bearings it can be stated that the yaw misalignment (side winds), individual blade pitching (pitch angle deviation) and wind speed during operation (wind speed distribution) are the most dominant influences in the load profile and life time calculation of main bearings.

3.3. Tower head loads due to rotor hub loads

After discussing the blade root (pitch bearing) and hub (main bearing) loads in the previous two subsections, finally the tower head loads are considered. These are equivalent to the yaw system loads since the main bearings are fixed on the steel base frame (nacelle) which is installed on the top of the tower. The loads of the steel base frame are transmitted via the yaw system to the tower head. Therefore, the rotor hub loads are also handled by the yaw system and tower (cp. Fig. 20). The top of the tower has to absorb both wind rotor loads and gravity forces caused by masses of nacelle and drive train components like gearbox, generator and others. In this section the tower head loads due to the rotor hub loads are calculated. The mass gravity forces of nacelle and different drive train components are again neglected. Based on Fig. 20, the tower head force and moment are defined as follows:

$$\vec{F}_{tower} = \vec{F}_{hub} = \begin{pmatrix} F_{hub,x} \\ F_{hub,y} \\ F_{hub,z} \end{pmatrix} \tag{48}$$

$$\vec{M}_{tower} = \vec{l}_{rotor} \times \vec{F}_{hub} + \vec{M}_{hub} = \begin{pmatrix} l_{rotor} \\ 0 \\ 0 \end{pmatrix} \times \begin{pmatrix} F_{hub,x} \\ F_{hub,y} \\ F_{hub,z} \end{pmatrix} + \begin{pmatrix} i_G \cdot M_{hub,x} \\ M_{hub,y} \\ M_{hub,z} \end{pmatrix} \tag{49}$$

Note that the moment around the x-axis is the torque generated in the rotor shaft and the moment around the z-axis is the torque generated in the tower structure (to be counterbalanced by the yaw

Table 7
Equivalent load and main bearing life time for $v_{wind} = 12$ m/s.

Parameter setting	$L_{eq.}$ at $v_{wind} = 8.5$ m/s	$L_{eq.}$ at $v_{wind} = 12.0$ m/s	$(1/L_{eq.})^3$ at $v_{wind} = 12$ m/s	Δ life time [%]
h-t6°	1.000	1.000	1.000	0.00
y -3.0°	1.027	1.082	0.790	−21.02
y + 3.0°	0.983	0.952	1.158	15.81
p -1.5°	1.013	1.050	0.865	−13.52
p + 1.5°	0.989	0.975	1.079	7.93
turb. 5%	1.001	1.003	0.0991	−0.94

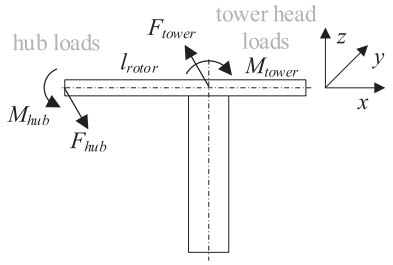

Fig. 20. Tower head loads due to rotor hub loads.

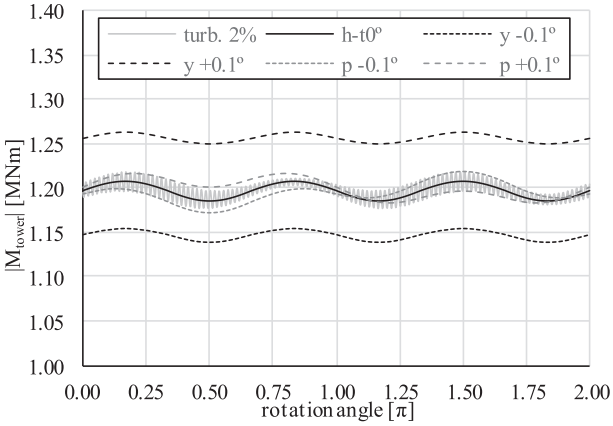

Fig. 21. Absolute value of tower head moment for the scenario in Table 4.

system). The torque ratio i_G is determined by the design of the gearbox and generator. For a drive train with a gearbox the ratio i_G depends on the number of planetary gear steps, the ratio of each planetary gear step as well as the total gearbox ratio. In the case of a direct drive train the ratio i_G is equal to one which means that the full torque generated in the rotor main shaft has to be balanced by the tower.

In order to compare the different scenarios of Tables 4 and 5, the tower head moment from Eq. (49) is evaluated. Figs. 21 and 22 show the absolute values of tower head moments calculated with the rotor to tower center distance $l_{rotor} = 1.25m$ (cp. Fig. 20). As the neglected gravity forces of rotor hub, main shaft, gearbox, generator and other tower head components are equivalent to a load offset, the tower head moment from Eq. (49) can be considered as the dynamic (fluctuating) part of the tower head loads. First, one can see from Fig. 21 an 22 that the change of both tilt and cone angle from 0° to 6° increases the tower head moment by a factor of approximately five. Consequently, the tilt and cone angle selection during the wind turbine design also has a significant influence on the tower head moment and thus, on the tower bending or tower torsion during operation. Second, depending on the side wind direction and yaw misalignment a negative or positive offset is caused on the tower head moment. Third, individual blade pitching, i.e. a pitch angle deviation of one blade increases the amplitude of the fluctuating tower head loads. Consequently, the dynamic peak loads of the tower head also increase due to individual pitching. Fourth, a frequency shift of the tower head loads from the third to the first rotor harmonic is observed (cp. Fig. 22: *h-t6°* versus $p + 1.5^{o}$) because of the reasons which were already explained in section 4.2. The frequency of the dynamic tower head loads can again be obtained from the product of the main shaft frequency and number of blades. Tower measurements [28] showed that the tower head is, in fact, excited by the third harmonic (three bladed

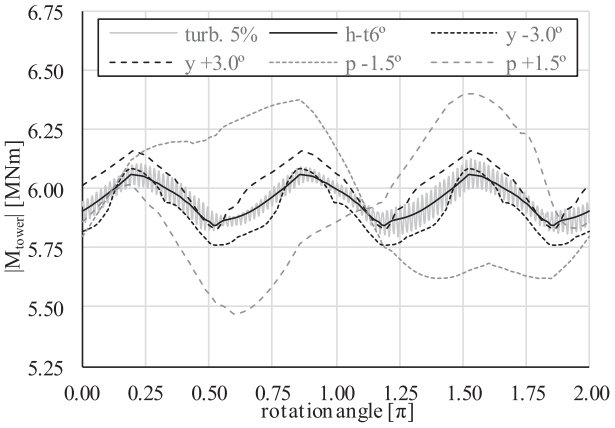

Fig. 22. Absolute value of tower head moment for the scenario in Table 5.

rotor). Fifth, it is also clear from Figs. 21 and 22 that load fluctuations due to wind turbulences are visible in the dynamic loads of the tower head and, again, lead to increasing peak values as well as load frequency.

In summary, the yaw misalignment (side winds) causes an offset of the tower head loads. Pitch angle deviation increases the dynamic loads of the tower and, in addition, shifts the load frequency to lower wind turbine rotor harmonics. For the tower behavior the increase of dynamic loads and a frequency shift of the tower head loads are more critical than a load offset. Therefore, the surface roughness (wind speed over height) and individual blade pitching (pitch angle deviation) are more critical for the tower than yaw misalignment or side winds.

4. Verification and discussion

Now, after the proposed method for calculating wind turbine components has been introduced and demonstrated, some issues remain for discussion. The most important issue is the verification of the load calculations, so that will be addressed first. To do so, the equivalent bearing load calculation results of section 3.2 are compared with measurements. However, loads (forces and moments) at the rotor hub and main bearings cannot directly be measured. An alternative way to evaluate the wind turbine rotor and main bearing loads is to consider the main shaft response to loads. The response to loads acting at one shaft end can be quantified by measuring the shaft displacement at the other shaft end assuming that the system is acting as a rigid body, not flexible. This assumption is justified because any rotating system should always run far from its resonance frequencies in order to protect it from its self-destruction. So based on the rigid body assumption, the response of the rotor hub loads can be measured as displacement at the gearbox or direct drive generator rotor. If, in addition, the main shaft loads (rotor hub loads) and load response are only compared from a qualitative point of view, then the exact shaft geometries are unimportant for the verification of the load calculation. This means that only normalized shaft displacements are compared. Without the requirement of detailed shaft geometries and bearing positions, existing displacement measurements can be used for the verification procedure. Gearbox displacements were already measured by Ref. [29] at a three bladed rotor with a known pitch angle deviation of 1.2° at one blade. In order to compare these measured gearbox displacements with the equivalent bearing load calculated with Eq. (45), the load calculations are executed with the parameter setting shown in Table 8. The calculation results are plotted in Figs. 23 and 24. Fig. 24 also includes the gearbox displacement measurements

Table 8
Parameter setting for main bearing (B1) load calculations.

Parameter setting	Surface roughness	Yaw angle ε	Pitch angle β	$\gamma_{tilt}/\delta + \gamma_{tower}$	Turbu-lences
L: p -1.2°	0.03	0°	−1.2°	5° + 2°	±2.5%
L: p + 1.2°	0.03	0°	+1.2°	5° + 2°	±2.5%

done by Ref. [29]. Both the calculated main bearing loads and measured displacements have been normalized by its average value and evaluated over one rotor rotation. Furthermore, the loads in *x'* (axial), *y'* (lateral) and *z'* (vertical) direction are plotted separately. By comparing Figs. 23 and 24, one can see that the load patterns in *x'*, *y'* and *z'*-direction, and thus the shaft displacement, are different for negative and positive blade pitching (cp. *Lz'*, *Ly'*, *Lx'* plotted in Figs. 23 and 24). In Fig. 24, it is also visible that the measured lateral (*Sy': p 1.2°*) and vertical (*Sz': p 1.2°*) gearbox displacement matches quite well with the calculated and normalized bearing load patterns *Ly' p + 1.2°* and *Lz' p + 1.2°*.

In summary, based on the gearbox displacement measurements and calculated load patterns plotted in Fig. 24, it can be concluded that the calculation methods proposed and used in the present paper adequately reflect the actual load patterns and profiles of a real wind turbine. Only the absolute values of the calculated loads could not be validated yet, as the required measurements are not (yet) available.

Now the model has been verified, some other aspects of the proposed approach will be discussed. The final aspect will be a comparison with the more commonly applied machine learning approaches.

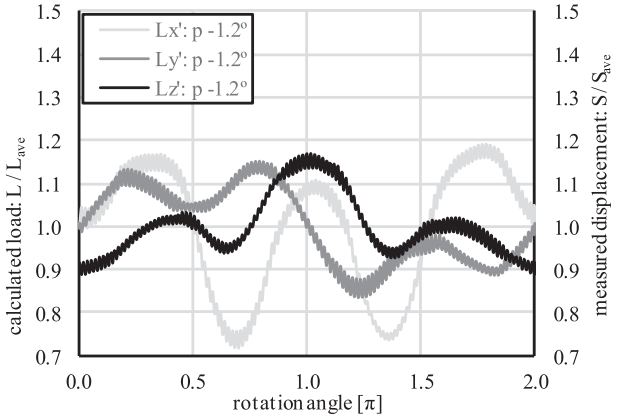

Fig. 23. Normalized calculated bearing (B1) loads (L) with pitch angle of −1.2°.

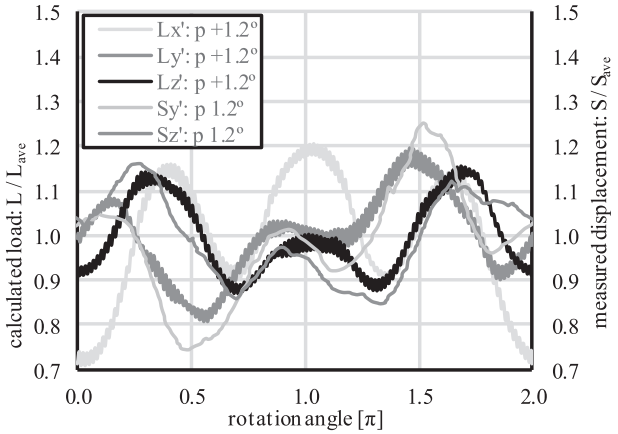

Fig. 24. Normalized calculated bearing (B1) loads (L) and normalized measured gearbox displacement (S) with pitch angle of +1.2°.

First, it was shown that the load profiles at blade root and pitch bearing are considerably affected by inertial forces, i.e. especially by Euler and Coriolis forces. By knowing that Euler and Coriolis forces occur in rotating (coordinate) systems, it can be concluded that the mass forces, i.e. gravity, centrifugal, Euler and Coriolis do not determine only the load profile of the blade and pitch bearing but also the load profile of all components and parts installed in the rotor hub of the wind turbine. Consequently, all components of the pitch system located in the rotor hub are affected by Euler and Coriolis forces, too. This means that a pitch system realized by hydraulic cylinders and tubes must counter act Coriolis forces because these forces occur as soon as the hydraulic cylinders move and oil is pumped through the tubes (moving mass). On the other hand, a pitch system utilizing a gearbox and electrical motor must handle centrifugal and Euler forces because all rotating parts of the gearbox and electrical motor do not only have an angular speed but also an angular acceleration during every pitch cycle. One can see from this consideration, that the load profiles (and life time) of the pitch system are not only determined by aerodynamic loads (airfoil moment) but also by mass forces in the rotating (coordinate) system of the rotor hub, number of pitching cycles and pitching velocity of rotor blades. In addition, it is important to note that active stall control introduces higher loads to both rotor blades and pitch system than a regular pitch control policy. The active stall control increases the turbulences on the suction side of the blade [19]. Therefore, the blade tends to flap more often and faster. Furthermore, active stall control rises the aerodynamic airfoil moment which, again, must be absorbed by the pitch system (hydraulic cylinder or gearbox).

Second, from Fig. 24, it is visible that the dynamic rotor hub loads can be evaluated by measuring the displacement of the gearbox housing. This means that the rotor hub loads also affect the load profiles of gearbox bearings and gears of the first gear step (which is realized as planetary gear set in nowadays wind turbines). Consequently, the life time of all bearings, shafts and gears of the first planetary gear set in a wind turbine gearbox are influenced by the rotor hub loads. Furthermore, as the rotor hub loads cause a dynamic gearbox displacement, the rotor hub loads also affect the output shaft (high speed shaft) of the gearbox. The dynamic gearbox displacement, during operation, increases the shaft end misalignment between gearbox and generator. An increasing misalignment of shaft ends reduces the life time of all high speed shaft bearings both on gearbox and generator side. If a direct drive generator is installed on the main shaft instead of a gearbox, then rotor hub loads cause a dynamic displacement of the generator rotor. In other words, due to the rotor hub loads the rotor-stator gap of the direct drive generator varies. Because of the fluctuating rotor-stator gap the magnetic flux density varies locally and thus the current in the generator stator. The fluctuating current and current peaks must, again, be handled by the full-scale power converter i.e. by capacitors, inductors as well as semiconductors like diodes and IGBTs.

Third, the tower head loads do not only bend the tower but also excite the complete turbine structure with the third or first harmonic of the wind turbine rotor. As the wind turbine rotor typically

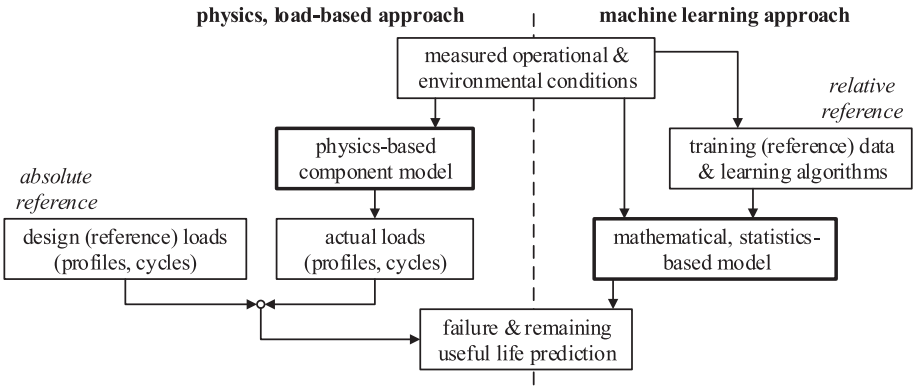

Fig. 25. Comparison of machine learning (data driven) and physics, load-based approaches.

rotates with an angular speed of 6–15 rpm i.e. 0.10–0.25 Hz, the turbine structure is excited by a frequency of approx. 0.1 Hz–0.75 Hz depending on rotor speed (wind speed) and pitch angle deviation. Therefore, it may occur that the wind turbine structure and substructures operate close to or even at their natural frequencies. Moreover, the tower head loads must also be handled by the yaw system because the yaw system transmits the rotor hub loads to the tower head. This means that the azimuth gear and their drives (i.e. gearboxes, brakes and electrical motors) must absorb the tower head moments. Therefore, the loads due to the tower head moments are significant for the life time prediction of the yaw system.

From these considerations, it can be seen that the load profiles of rotor hub center and tower head are crucial for the life time prediction of wind turbines. For a more accurate life time prediction it is useful to calculate load profiles and predict life time based on measurements, namely: wind speed at two different heights (second wind speed used for evaluation of surface roughness), wind speed distribution, side (and shear) winds, yaw misalignment, pitch angle deviations, number of blade flaps, blade flapping speed and average wind turbulence intensity. Then, based on the set of equations proposed in the present paper the load profiles of different wind turbine components can be calculated and therefore, the life time. By integrating the calculated load profiles and failure statistics it is possible to evaluate the life time under various environmental conditions. Moreover, the reduction of rotor hub loads is important in order to obtain an optimum life time. The rotor hub loads can be influenced either by the tilt and cone angle during the design procedure or by pitch and yaw control algorithms during operation. The control algorithms should reduce the pitch angle deviation and yaw misalignment during operation in order to lower load peaks at hub center (cp. Fig. 19) and tower head (cp. Fig. 22). Furthermore, blade pitching and nacelle yawing should be as smooth as possible to avoid or, at least, minimize Euler and Coriolis accelerations on blade and wind turbine rotor masses. A smooth blade pitching, however, stands in conflict with over speeding of the power train. This means that any load variation introduced into the wind turbine from the blades or rotor hub does affect the load (and associated life time) of many components of the complete wind turbine. It is, therefore, crucial for the wind turbine asset management to understand and quantify these interactions.

Finally, the proposed physics-based approach for life prediction is compared to the more commonly adopted data-driven approach. As was mentioned in the introduction (section 1), this load-based maintenance approach does not only allow failure and remaining useful life (RUL) predictions with higher accuracy but also enables these predictions at an early moment when the component (system) is still “healthy”. The higher accuracy is obtained because specific and representative physical component models (like virtual wind turbine blades) are used for evaluating the actual loads (at blade root, hub center and tower head) and because these actual loads are compared with design loads (like bearing load capacities). The early prediction is possible because there is no need to wait for actual failures or anomalies to occur. This means that once the component has run through the range of these operational and environmental conditions, the load profiles are known and the RUL can be evaluated. These are clear advantages in comparison to commonly used data driven or machine learning approaches which use mathematical, statistics-based models trained by learning algorithms and reference data sets [30]. The mathematical, statistics-based models are used to identify deviations from normal operational conditions (anomaly detection) and to predict failures and the RUL. This means that the prediction i) is based on a relative reference because the relation between the training data set and the design life time (absolute reference) is unknown and ii) can only be done after a certain number of failures has occurred or clear changes of operational conditions can be measured. The principle of both approaches are visualized in Fig. 25. However, it must also be mentioned here that the higher accuracy and early prediction of the physics and load-based approach are at the expenses of more detailed information on components (e.g. geometries, dimensions, bearing types, etc.) and on the operational and environmental conditions. Therefore, the comparison of the two approaches also demonstrates that the more detailed the input data and prediction model are, the earlier and more accurate predictions are possible.

5. Conclusion and outlook

In the present paper a model and method is introduced for load-based maintenance on a three bladed, horizontal axis, upwind wind turbine. A calculation procedure was proposed to evaluate loads (forces and moments) at blade roots, rotor hub center and tower head during wind turbine operation. The dominant influences in the load profiles were detected by performing load sensitivity analyses for different scenarios and parameters. Table 9 summarizes the results by providing an overview of critical parameters and their effects on load profiles. The influences are categorized in neutral, minor and major. It is recommended to consider, at least, minor and major influences when the load profiles for a specific wind turbine are calculated.

Moreover, measurements are needed to specify and take properly into account the dominant parameters in the load profile calculation. Table 10 gives an overview of the measurements which are required to calculate the load profiles. These measurements

Table 9
Overview of critical/dominant calculation parameters.

Parameter	Blade root loads	Hub (tower) loads	Load effect for 3 bladed rotor
Tilt, cone angle	minor	major	– High load increase – Load offset due to increasing load unbalance
Side/(shear) wind, yaw misalignment	neutral	minor	– Load offset
Pitch angle deviation	minor	major	– Increase of dynamic peak loads – Shift of load frequency from 3rd to 1st rotor harmonic
Surface roughness	neutral	minor	– Dynamic loads with 3rd rotor harmonic (3 blades)
Turbulences (wind gusts)	neutral (major)	neutral (minor)	– Neutral: small/even distributed turbulences – Minor/major: gusts, blade flapping
Mass forces	major	neutral	– neutral: initial coordinate system, mainly load offset – major: rotating coordinate system, Coriolis force due to blade flapping
Wind speed (distribution)	major	major	– loads proportional to square of wind speed (if $v_{wind} < v_{wind,\ rated}$)

Table 10
Overview of required measurements for load-based life time prediction.

Load profile evaluation at/Life time of	require measurements of/is determined by
– blade (root) – pitch bearing	– angular main shaft speed – number of blade flaps – blade flapping velocity – number of blade pitches – blade pitching velocity
– pitch system (installed in rotor hub)	– angular main shaft speed – number of blade flaps – blade flapping velocity – number of blade pitches – blade pitching velocity – wind speed – wind speed distribution
– rotor hub center – main bearings – gearbox + generator – direct drive generator – yaw system – tower (head)	– wind speed – wind speed distribution – wind speed over height – side/shear winds – yaw misalignment to main direction of wind speed – pitch angles respectively pitch angle deviations – wind gusts – wind turbulence intensity

were derived from the sensitivity analyses performed in the present paper. Further, the present paper focused specifically on the calculation of load profiles under operational conditions because the resulting accurate load profiles can both enable more efficient maintenance of the system and lead to a better system design.

To give a short outlook into future application of this concept in real wind turbines, three different ways of life time prediction can be distinguished. First, the most accurate way to predict the life time is the calculation of both load profiles and life time based on measurements and given component dimensions. This approach was exemplary shown and applied to main shaft bearings in section 3.2 and can also enable designers to improve their designs, because they know what loads components must bear in operation. Second, if the life time cannot be calculated, e.g. due to missing information, then a relation can be created between load profiles, number of operating hours and failure statistics. The evaluated relation is then used to predict the life time. Third, if neither the life time nor the load profiles can be calculated, then a relation between measurements of the dominant influences in the load profiles, operating hours and failure statistics can be found. The detected relation, again, is utilized to estimate the life time or number of load cycles. So it can be concluded that the evaluation and measurement of the dominant influences in the load profiles are essential for life time prediction of wind turbine components during both maintenance and design.

Finally, future works may combine the approach of physics-based component model and load-based failure prediction shown in this paper with wind turbine control designs [31] and signal processing [32] to improve the performance of wind turbine systems.

Acknowledgment

This work was part of the Wind turbine Maintenance and Operation decisions Support (WiMOS) project. The project has been funded and supported by TKI Wind op Zee, IX Wind and Joulz Energy Solutions.

References

[1] B. Maples, G. Saur, M. Hand, R. van Pietermen, T. Obdam, Installation, operation, and maintenance strategies to reduce the cost of offshore wind energy, Tech. Rep. (2013) 1–106. Nrel/Tp-5000-57403, no. July.
[2] M. Asgarpour, J.D. Sørensen, State of the art in Operation and Maintenance planning of offshore wind farms, in: Safety and Reliability: Methodology and Applications - Proceedings of the European Safety and Reliability Conference, ESREL 2014, 2015.
[3] J. Ribrant, L.M. Bertling, Survey of failures in wind power systems with focus on Swedish wind power plants during 1997-2005, IEEE Trans. Energy Convers. 22 (1) (2007) 167–173.
[4] C. KAIDIS, Wind Turbine Reliability Prediction a Scada Data Processing & Reliability Estimation Tool, 2013, pp. 1–72, no. September.
[5] M. Canizo, E. Onieva, A. Conde, S. Charramendieta, S. Trujillo, Real-time predictive maintenance for wind turbines using Big Data frameworks, in: 2017 IEEE Int. Conf. Progn. Heal. Manag. ICPHM 2017, 2017, pp. 70–77.
[6] Y. Zhao, D. Li, A. Dong, D. Kang, Q. Lv, L. Shang, Fault prediction and diagnosis of wind turbine generators using SCADA data, Energies 10 (8) (2017) 1–17.
[7] J. Herp, M.H. Ramezani, M. Bach-Andersen, N.L. Pedersen, E.S. Nadimi, Bayesian state prediction of wind turbine bearing failure, Renew. Energy 116 (2018) 164–172.
[8] M. Asgarpour, J. Sørensen, Bayesian based diagnostic model for condition

based maintenance of offshore wind farms, Energies 11 (2) (2018) 300.
[9] Y. Hu, et al., A prediction method for the real-time remaining useful life of wind turbine bearings based on the Wiener process, Renew. Energy 127 (2018) 452–460.
[10] Z. Tian, T. Jin, B. Wu, F. Ding, Condition based maintenance optimization for wind power generation systems under continuous monitoring, Renew. Energy 36 (5) (2011) 1502–1509.
[11] L. Vera-Tudela, M. Kühn, Analysing wind turbine fatigue load prediction: the impact of wind farm flow conditions, Renew. Energy 107 (2017) 352–360.
[12] C.S. Gray, S.J. Watson, Physics of failure approach to wind turbine condition based maintenance, Wind Energy 13 (2010) 395–405.
[13] T. Tinga, Application of physical failure models to enable usage and load based maintenance, Reliab. Eng. Syst. Saf. 95 (10) (2010) 1061–1075.
[14] M. Engeler, D. Treyer, D. Zogg, K. Wegener, A. Kunz, Condition-based maintenance: model vs. Statistics a performance comparison, Procedia CIRP 57 (2016) 253–258.
[15] M.A. Djeziri, S. Benmoussa, R. Sanchez, Hybrid method for remaining useful life prediction in wind turbine systems, Renew. Energy 116 (2018) 173–187.
[16] S.S. Gokhale, K.S. Trivedi, Analytical modeling, Encycl. Distrib. Syst. (1998).
[17] M.O.L. Hansen, Aerodynamics of Wind Turbines, second ed., Taylor & Francis, 2013.
[18] S. Gundtoft, Wind Turbines (2009).
[19] T. Burton, N. Jenkins, D. Sharpe, E. Bossanyi, Wind Energy Handbook, 2011.
[20] EUROS, Blade Family EU90 | 100, 2009.
[21] N. Timmer, Airfoil Data of NACA 64-618, DU 93-W-210ML, DU 97-W-300LM, Excel Sheet, 2009. Delft, The Netherlands.
[22] E. Hau, H. von Renouard, Wind Turbines: Fundamentals, Technologies, Application, Economics, Springer Berlin Heidelberg, 2005.
[23] K.H. Grote, E.K. Antonsson, Springer Handbook of Mechanical Engineering, vol 10, Springer, 2009.
[24] J.F. Manwell, J.G. McGowan, A.L. Rogers, Wind Energy Explained: Theory, Design and Application, Wiley, 2010.
[25] DIN ISO 281, Rolling Bearings - Dynamic Load Ratings and Rating Life - Calculation Methods, 2009.
[26] F.D. Bianchi, H. de Battista, R.J. Mantz, Wind Turbine Control Systems: Principles, Modelling and Gain Scheduling Design, Springer London, 2007.
[27] FAG, Wälzlager Hauptkatalog, Schweinfurt, Schaeffler KG, 2008.
[28] W. Hu, S. Said, A. Multibrid, N. Sea, Resonance phenomenon in a wind turbine system under operational conditions 1,2,3,4, in: 9Th Int. Conf. Struct. Dyn, 2014.
[29] A. Heege, J. Hemmelmann, L. Bastard, J.L. Sanchez, L. Lens, M. Omiciuolo, Matching Experimental and Numerical Data of Dynamic Wind Turbine Loads by Modelling of Defects, vol. 3, 2009.
[30] A. Stetco, et al., Machine learning methods for wind turbine condition monitoring: a review, Renew. Energy 133 (2019) 620–635.
[31] A.D. Wright, L.J. Fingersh, Advanced control design for wind turbines Part I : control design, implementation, and initial tests, Tech. Rep. Natl. Renew. (2008) 98. Energy Lab., no. March.
[32] S. Simani, P. Castaldi, Adaptive signal processing strategy for a wind farm system fault accommodation *, IFAC-PapersOnLine 51 (24) (2018) 52–59.